

## Research paper

## Factors controlling margin instability during the Plio-Quaternary in the Gela Basin (Strait of Sicily, Mediterranean Sea)

Tugdual Gauchery<sup>a</sup>, Marzia Rovere<sup>a,\*</sup>, Claudio Pellegrini<sup>a</sup>, Antonio Cattaneo<sup>b</sup>, Elisabetta Campiani<sup>a</sup>, Fabio Trincardi<sup>a</sup>

<sup>a</sup> Istituto di Scienze Marine, National Research Council, Via P. Gobetti 101, 40129, Bologna, Italy

<sup>b</sup> IFREMER, Géosciences Marines, Z.I Pointe du Diable, BP70, Plouzané, France



## ARTICLE INFO

## Keywords:

Stratigraphy  
Middle Pleistocene Transition  
Plio-Quaternary  
Contourites  
Climothems  
Mass-transport deposits  
Continental margin evolution  
Glacio-eustatic variations

## ABSTRACT

This study presents novel findings on the Pliocene and Quaternary evolution of the Gela Basin (Strait of Sicily, Mediterranean Sea), an area recording the interaction between tectonics, climate change at Milankovitch and sub-Milankovitch timescales, and dynamic water masses exchange between the eastern and western Mediterranean Sea. The calibration of seismic profiles with exploration boreholes allowed for the refining of the chronostratigraphic framework of the Gela Basin and highlighted the main phases of margin growth. Since the Pliocene, the margin has recorded the deposition of 100 m high shelf-edge clinothems, accompanied by sediment drifts on the slope and mass-transport deposits (MTDs), possibly triggered by seismic activity. Through the Plio-Quaternary the locus of deposition of sediment drifts migrated upslope due to a progressive shift of bottom currents. After the Middle Pleistocene Transition (MPT) the margin experienced an accelerated outbuilding with the deposition of a 700 m thick succession in only 0.8 Myr. At this time, a marked change in sedimentary architecture reflects the growth of shelf-edge clinothems and associated MTDs on the slope, and the spreading of contourite deposits over a broader and generally shallower area. Sediment flux to the basin and the intensity of bottom currents appear both paced at 100 kyr eccentricity orbital cycles. The growth of bottom current deposits on a large portion of the upper slope and outer shelf likely reflects constraints to the bottom current flow by the margin morphology, inherited from Miocene and Pliocene tectonics. Overall, a combination of long-term tectonic activity, climate change and shifts in oceanographic regime resulted in a complex along-strike variability of the margin morphology and stratigraphic architecture and affected where and when MTDs were emplaced. These conclusions show how climate cyclicity influence sediment supply which combined with margin morphology can promote slope instability in continental margins.

### 1. Introduction

Continental margins preserve a unique long-term sedimentary record that offers the opportunity to study changes in eustasy (Tziperman and Gildor, 2003), modified by local tectonic-driven uplift/tilting/subsidence of the margin, sediment supply (Llave et al., 2011) and oceanographic regime (Thiéblemont et al., 2019). Stratigraphic successions therefore reflect a combination of changing climate, oceanographic regime and tectonic conditions (e.g. Gong et al., 2018; Pellegrini et al., 2020; Steckler et al., 1998). Stratigraphic successions represent ideal archives to solve: i) variation in strata geometries as physical expressions of long-term climatic components; ii) relation between climate regime, tectonic activity and fluctuations in sediment flux from

catchment(s) to the basin; iii) impact of glacio-eustatic cycles on the processes that govern how the sediment is delivered, transported, deposited and ultimately remobilized into the basin.

A variety of sedimentary bodies may deposit and coexist along a continental margin, including clinothems, turbidite, mass-transport (MTDs) and contourite deposits (e.g. Anell and Midtkandal, 2017; Faugères et al., 1999; Johannessen and Steel, 2005; Paumard et al., 2019). The Pliocene and Quaternary are ideal time intervals to study these sedimentary bodies; specifically after the Middle Pleistocene Transition (MPT), high-amplitude (ca. 120 m) fluctuations caused variations in sediment supply and played a crucial role in continental margin outbuilding (Somoza et al., 1997). These fluctuations forced systematic shifts in the position of the shoreline across the continental

\* Corresponding author.

E-mail address: [m.rovere@ismar.cnr.it](mailto:m.rovere@ismar.cnr.it) (M. Rovere).

<https://doi.org/10.1016/j.marpetgeo.2020.104767>

Received 6 February 2020; Received in revised form 9 October 2020; Accepted 14 October 2020

Available online 22 October 2020

0264-8172/© 2020 The Authors.

Published by Elsevier Ltd.

This is an open access article under the CC BY-NC-ND license

(<http://creativecommons.org/licenses/by-nc-nd/4.0/>).

shelves, resulting in progradational, retrogradational and aggradational stratal stacking patterns (Patrino and Helland-Hansen, 2018). In these contexts, clinoforms and clinothem (clinoform-bounded sedimentary units) represent fundamental building blocks of the margin characterized by different geometric elements with a topset (low angle, shallow sector), a foreset (steepest angle and dip seaward) and a bottomset (low angle, deep sector) (Steel and Olsen, 2002). In addition, the MPT was likely accompanied by a global reorganization of the thermohaline circulation (Pena and Goldstein, 2014) with enhanced deposition of contourite systems after the MPT, as documented along the Atlantic-Mediterranean water mass exchange, with the more saline Mediterranean Water Outflow affecting the Algarve margin in the Gulf of Cádiz (Roque et al., 2012) and the Cantabrian margin in the NE Atlantic (Van Rooij et al., 2010). Similarly, in the Mediterranean Sea, thermohaline circulation enhanced contourite deposition after the MPT in the Corsica Trough (Miramontes et al., 2016), the southwestern Adriatic margin (Pellegrini et al., 2016) and the Balearic Promontory (Vandorpe et al., 2011).

The higher rates of sediment accumulation during the Pleistocene resulted in high rates of deposition and caused mass movement of sediments that were deposited too rapidly to allow for stable accumulation along the slopes. While submarine mass failures are indeed well-known along the fronts of rapidly prograding depositional systems from deltas to continental slope settings (Thöle et al., 2016), other studies have investigated the relationships between contourite deposits and MTDs (Laberg and Camerlenghi, 2008; Martorelli et al., 2016; Miramontes et al., 2018; Stoker and Hafliðason, 2005). However, the role of contourite deposits on margin stability is not yet fully understood.

Here, we document the case of a sector of the Mediterranean

continental margin, the Gela Basin (GB), characterized by the deposition of clinothem, contourite deposits and MTDs through the Plio-Quaternary. The added value in studying the GB is threefold: 1) its location in the Strait of Sicily is a key area of water masses circulation and exchange between the Atlantic Ocean and the eastern and western Mediterranean Sea; 2) its limited extent (90 km along-strike) offers the opportunity to study the variability of stratal geometries and margin morphology; 3) it has relatively high sedimentation rates which allow to study the effect of long-term climate change on different depositional systems.

In this study, we focus on the eastern side of the basin and document: 1) the predominance of tectonics as a predisposing factor for margin instability during the Pliocene; 2) the onset of contourite deposits and their role in favouring slope instability from the Late Pliocene, as an additional predisposing factor for slope failure; and 3) climate variability as the main driver of stratigraphic architecture and margin instability after the MPT.

## 2. Background

### 2.1. Geodynamic and tectonic setting of the Gela Basin

The Gela Basin (GB), located in the northern Strait of Sicily (Fig. 1), represents the Pliocene-Quaternary foredeep of the Maghrebic fold-and-thrust belt, which developed at the subduction-collisional boundary between the European and African plates (Colantoni et al., 1975). In the north, the GB was overthrust during the late Pliocene–early Pleistocene by the southern movement of the Gela Nappe, the southernmost migrating thrust wedge of the Maghrebic chain (Argnani,

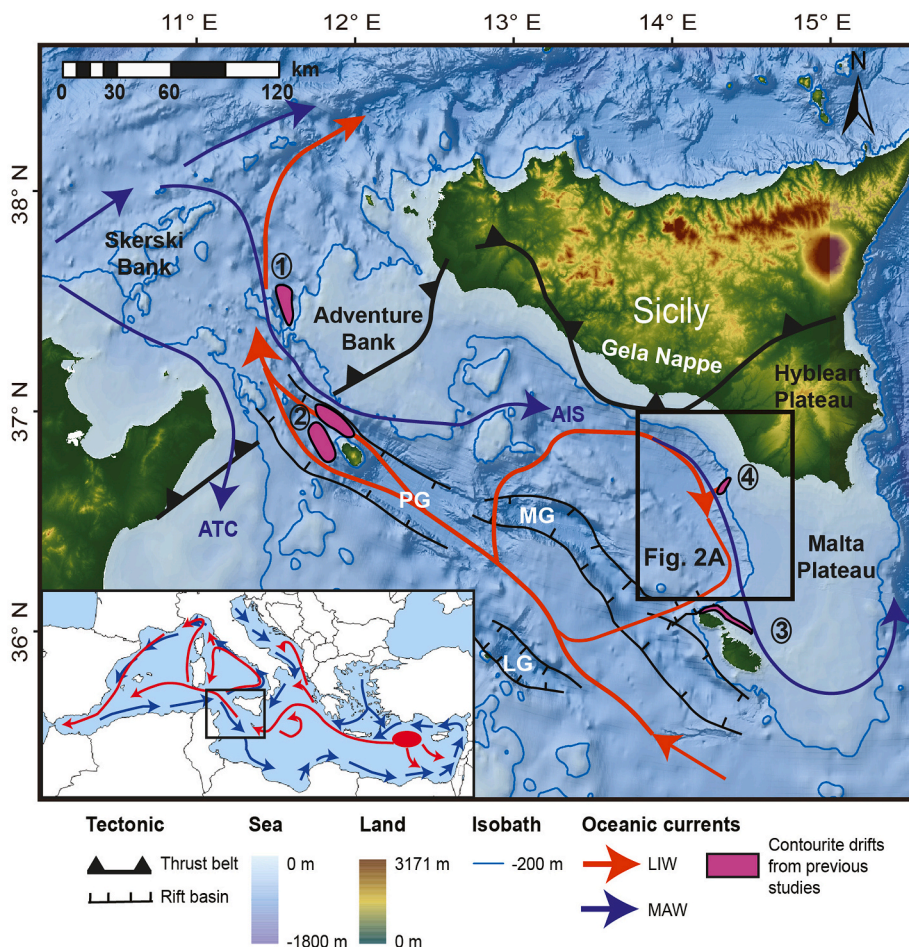


Fig. 1. Relief and bathymetric map of the Strait of Sicily; red and blue arrows represent the Levantine Intermediate Water (LIW) and the Modified Atlantic Water (MAW) (adapted from Lermusiaux and Robinson, 2001). 1–4 = previously studied contourite deposits: 1 = Marani et al. (1993), 2 = Martorelli et al. (2011), 3 = Micallef et al. (2013) and 4 = Verdicchio and Trincardi (2008). AIS = Atlantic Ionian Stream, ATC = Atlantic Tunisian Current, PG = Pantelleria Graben, MG = Malta Graben, LG = Linosa Graben. Inset: general oceanographic circulation in the Mediterranean Sea. (For interpretation of the references to colour in this figure legend, the reader is referred to the Web version of this article.)

1987; Butler et al., 1992). The Maghrebian fold-and-thrust belt reached its current position during the middle–late Pleistocene, concomitantly to a general uplift of the Hyblean Plateau (Ghielmi et al., 2012). The GB is delimited in the south and southwest by a NW–SE trending extensional rift system comprised of banks and grabens (Finetti, 1984, Fig. 1). The rift system formed in the late Miocene to early Pliocene, continued through the Quaternary forming the deep (> 1000 m) Pantelleria, Malta, and Linosa grabens (Gardiner et al., 1995, Fig. 1). Normal faults belonging to the same extensional system extend across the GB, where they are buried below the late Pliocene–Quaternary sediment infill (Argnani, 1987; Ghisetti et al., 2009).

The GB is rimmed by a narrow (8 km) continental shelf in the north, broadening to several tens of kilometres in the 100–150 m deep Malta Plateau, a structural horst of the Pelagian African foreland (Bishop and Debono, 1996). Following the Africa–Europe collision, moderate inversion tectonics affected the Malta Plateau (Argnani and Torelli, 2001), and regional uplift occurred in late Pliocene between Malta and SE Sicily, generating NE-trending normal faults (Gardiner et al., 1995). The uplift may have favoured the development of westward-prograding Quaternary wedges observed on the western sector of the Malta Plateau (Ghielmi et al., 2012; Minisini et al., 2007).

## 2.2. Oceanographic circulation

The Mediterranean Sea is a semi-enclosed basin connected to the Atlantic Ocean through the Strait of Gibraltar (inset of Fig. 1). The oceanographic circulation in the Mediterranean Sea is mainly composed of the Modified Atlantic Water (MAW), a relatively fresh and light water from the Atlantic and the Levantine Intermediate Water (LIW), saltier and relatively warmer formed in the Levantine Sea (Béranger et al., 2004). The flow of these two water masses generates oceanic currents across the Strait of Sicily: the MAW, directed eastward at 0–200 m water depths (w.d.) and the LIW, flowing westward between 200 and 500 m w. d. (Lermusiaux and Robinson, 2001; Astraldi et al., 2001). On the western side of the Strait of Sicily, the MAW is partially deviated northward by the Skerki Bank and then split into three main branches (Astraldi et al., 2001, Fig. 1). The first branch directly flows into the Tyrrhenian Sea along the northern coast of Sicily, while the remaining two turn southward (Astraldi et al., 2001, Fig. 1). The Atlantic Tunisian Current (ATC) flows south of the study area at the edge of the Tunisian shelf along the 200 m isobath, while the Atlantic Ionian Stream (AIS) circulates in the GB and Malta Plateau (Lermusiaux and Robinson, 2001, Fig. 1). The path of the LIW is influenced by the seafloor morphology and, due to Bernoulli's effect, its flow speed in the Strait of Sicily

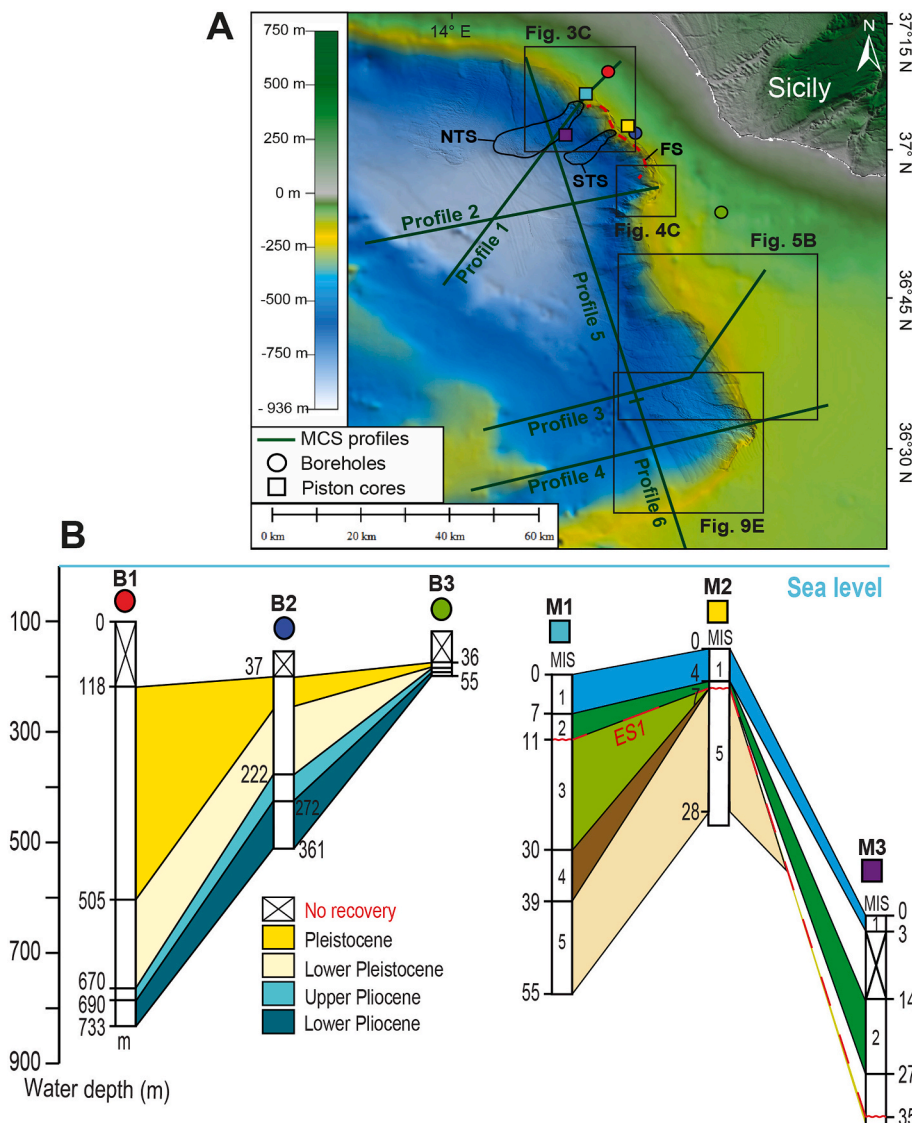


**Fig. 2.** A. The eastern Gela Basin bathymetric map showing the location of the MCS profiles (green lines), deep boreholes (circles) and piston cores (squares) used in this study. The deep boreholes cross section is on depositional strike, whether the piston core cross section is on depositional dip. NTS: Northern Twin Slide, STS: Southern Twin Slide, FS: Father Slide. B. Regional stratigraphic correlation between the boreholes B1–B3 and the piston cores M1–M3. See also Table 1. (For interpretation of the references to colour in this figure legend, the reader is referred to the Web version of this article.)

(Astraldi et al., 2001) increases in the GB (Lermusiaux and Robinson, 2001).

### 2.3. Stratigraphy and late Quaternary depositional sequences

A widespread shallow-water carbonate platform covered the Malta Plateau since the late Triassic and until the Oligocene. Since the Oligocene, clastic sediments started to spread over the Malta Plateau from the emerging Maghrebian fold-and-thrust belt. During the Messinian Salinity Crisis, when a regional desiccation event led to basin-wide accumulation of evaporitic and post-evaporitic deposits, a marked erosional unconformity formed across the margin (Base Pliocene in this study), overlain by 2.5 km of shallowing-upward Pliocene-Quaternary marine sediments (Colantoni et al., 1975).

Seismic stratigraphic analysis carried out in the western GB revealed several unconformity-bounded depositional sequences consisting of Pliocene and Pleistocene deposits up to 1.9 km thick in the deepest part of the basin (Di Stefano et al., 1993). On the shelf, well-developed prograding complexes correlating to turbidites in the basin characterize Pleistocene deposits (Di Stefano et al., 1993).

Two piston cores, 55 m and 27 m long, located at the shelf edge and on the slope of the northern GB (Fig. 2A), sampled almost entirely the sedimentary succession emplaced during the last 100 kyr glacio-eustatic cycle, spanning from Marine Isotope Stage 5 (MIS 5) to the Holocene (Kuhlmann et al., 2015 and Fig. 2B). Radiocarbon dates bracket the hiatus associated with the Erosional Surface (ES1) between the Last Glacial Maximum (LGM) and ~30 kyr cal BP (Kuhlmann et al., 2015). Seismic reflection profiles across the coring sites indicate that the last phase of clinothem aggradation occurred during MIS 5. To explain the enhanced sediment accumulation rates (SAR) of up to 200 cm kyr<sup>-1</sup> during highstand conditions, an intensification of LIW activity associated with the flooding of the Malta Plateau and highlighted by the presence of contourite deposits was invoked (Kuhlmann et al., 2015).

### 2.4. Contourite deposits in the Gela Basin

Within the Strait of Sicily, Marani et al. (1993) first described contourite deposits along the Adventure Bank (Fig. 1). Small, mounded drifts and irregular patch drifts as well as zones of scours were described within the deep rift basins (Reeder et al., 2002) and around Pantelleria Island (Martorelli et al., 2011, Fig. 1). Shallow contourite deposits (< 300 m w. d.) were discovered in the upper slope of the northern GB (Verdicchio and Trincardi, 2008a, b; Fig. 1) and along the northern coast of Malta (Micallef et al., 2013). Well-defined contour-parallel elongated moats (700 m wide and 50 m deep) possibly developed in response to the LIW flow along the shelf edge (Verdicchio and Trincardi, 2008a).

### 2.5. Mass-transport deposits in the Gela Basin

Several mass-transport deposits (MTDs) were highlighted by previous studies in the northern part of the basin. The Gela Slide, with a thickness of 700 m and an inferred volume of 1050 km<sup>3</sup>, was probably emplaced 600 ka (Di Stefano et al., 1993), likely involving the surface slope of the frontal area of the Gela Nappe (Trincardi and Argnani, 1990).

Slope instability after the early Pleistocene affected progradational sequences characterized by a progressive steepening (Minisini and Trincardi, 2009). A large MTD (18.9 km<sup>3</sup>), named Father Slide (FS in Fig. 2A), was emplaced ~87 ka and involved MIS 5e to MIS 5c sedimentary units. The Father Slide was followed by eight major slope failure events with a ~10 kyr return frequency (Kuhlmann et al., 2017). In particular, during the late Holocene, frequent failures affected post-glacial unconsolidated deposits with the emplacement of two larger MTDs: the Northern Twin Slide with a volume of 0.57 km<sup>3</sup> and the Southern Twin Slide with a volume of 0.36 km<sup>3</sup> (Minisini et al., 2007; Minisini and Trincardi, 2009, Fig. 2A). In the late Holocene, mudflows

have also been observed in bathymetric data affecting the downslope flank of contourite deposits along the northern slope of the basin (Verdicchio and Trincardi, 2008a, b; Fig. 1).

Preferential failure planes for the largest MTDs are provided by surfaces at the base of the lowstand progradational wedge or at the base of the post-glacial contourite deposits (Minisini and Trincardi, 2009). Occasionally, they include volcanic ash layers (Kuhlmann et al., 2017). Rapid deposition of Quaternary units and progressively increasing slope angles of prograding units explain the frequent recurrence of slope failures in the Gela Basin (Kuhlmann et al., 2017).

## 3. Material and methods

### 3.1. Boreholes and sediment cores

Three deep industry boreholes located on the shelf (Fig. 2A) were used for core-seismic correlation, together with the information from three published long piston cores (M1 and M2 from Kuhlmann et al., 2015; M3 from Kuhlmann et al., 2017) (Fig. 2B, Table 1). The log data of the boreholes (Plinio Sud 001, Pellicano Ovest 001 and Merluzzo Mare 001; B1–B3 in Fig. 2B) recovered along the northern shelf (accessible online at <http://www.videpi.com/videpi/progetto.asp>) reached the Mesozoic by drilling 4332 m, 4524 m and 2906 m, respectively. In this study, we used the stratigraphic information from the Base of Pliocene, which represents the marine sedimentation after the Messinian Salinity Crisis; for sub-epochs, we used the informal spatial subdivision i.e. Lower, Middle, Upper (Haile, 1987; Pearson et al., 2017). Borehole “Plinio Sud 001” (B1 in Fig. 2) allowed us to correlate three key seismic reflections corresponding to: Lower Pliocene, Upper Pliocene and Lower Pleistocene. The reported taxa *Globorotalia bononiensis*, *G. puncticulata*, *G. margaritae* (rare), and *Sphaeroidinellopsis Sphaeroidinellopsis* sp. *Globogerinoides obliquus*, *G. extremus*, *G. sacculifer* (frequent), *G. trilobus*, *Orbulina universa* was equated to the time interval spanning the Mediterranean Pliocene (MPL) 1 (5.33 Ma) – MPL 4a (3.57 Ma) biozones (Lower to Early Middle Pliocene). The taxa *G. crassaformis*, *G. aemiliana*, *G. extremus*, *G. obliquus* are planktonic key taxa present in this interval, indicating an age not older than MPL 4b biozone (3.57 Ma) and not younger than MPL 5b biozone (2.09 Ma) (Upper Pliocene to Lower Pleistocene after Gibbard et al., 2010), according to Lirer et al. (2019) and references therein. The taxa *G. inflata* (frequent) and *G. extremus* (rare) correspond to MPL 6 biozone (2.09–1.79 Ma) (Lower Pleistocene after Gibbard et al., 2010) according to Lirer et al. (2019) and references therein. The last interval between 505 and 470 m shows planktonic taxa (*G. pachyderma*, *G. truncatulinoidea*, *G. inflata*) of Pleistocene age, from MPL 6b (2 Ma) to MPL e2e2 (present) biozone, according to the updated biochronology (Lirer et al., 2019).

### 3.2. Multi-channel seismic (MCS) reflection profiles

A set of unpublished MCS profiles (Fig. 2A) was made available by Eni S.p.A. and accessed through the virtual data room at their premises in San Donato Milanese (Italy). The interpretation software package used was Halliburton-Landmark Decision Space® G1 Edition. To interpret the stratigraphy of the margin, we identified reflection configurations and terminations, described the seismic facies (Table 2) and selected key unconformities in MCS profiles. On the shelf, these unconformities show an erosional character highlighted by top-lapping reflections and for this reason have been labelled Erosional Surfaces (ESs) in earlier works (ES1 and ES2; Kuhlmann et al., 2015; Minisini et al., 2007). Eight erosional surfaces (ES1–ES8) were thus identified on the topsets with ES8 coinciding with the MPT horizon traced and correlated at 800 ka in the northern GB by Di Stefano et al. (1993). The sequences above the erosional surfaces show overlapping terminations on the upper slope and pass basinward to correlative conformities (Fig. 6A).

The term clinoform denotes surfaces which gently prograde seawards (Rich, 1951) characterized by three geometric elements (topset,

**Table 1**  
Boreholes and sediment piston cores used in this study.

Core/ Borehole	Type	Total drilling depth (m)	Map key	Coordinates		Year	Operator	Water depth (m)	Length used (m)	Stratigraphy	comments	Reference
				Latitude	Longitude							
Plinio Sud 001	Well	4332	B1	36°53.607'N	14°16.232'E	1981	AGIP	100	733	Plio- Quaternary	missing Upper Quaternary	website Videpi
Pellicano Ovest 001	Well	4524	B2	36°47.46'N	14°19.042'E	1973	AGIP	145	370	Plio- Quaternary	missing Upper Quaternary	website Videpi
Merluzzo Mare 001	Well	2906	B3	36°39.387'N	14°27.83'E	1982	ELF	94	79	Plio- Quaternary	missing Upper Quaternary	website Videpi
GeoB14403	Piston core	55	M1	36°51.410'N	14°13.910'E	2010	MARUM	182	55	MIS 1 - MIS 2 - MIS 3 - MIS 4 - MIS 5		<a href="#">Kuhlmann et al. (2015)</a>
GeoB14414	Piston core	27	M2	36°48.130'N	14°18.170'E	2010	MARUM	146	27	MIS 1 - MIS 2 - MIS 5		
GeoB14401	Piston core	36	M3	36°47.20'N	14°11.90'E	2010	MARUM	613	36	MIS 1 - MIS 2	no recovery 3–15 m	<a href="#">Kuhlmann et al. (2017)</a>

**Table 2**  
Seismic facies F1 to F5 observed in MCS profiles, complemented with illustrative images, sketches, facies descriptions and inferred sedimentary processes.

Name	Image	Line drawing	Description	Sediment processes	Interpretation
F1			High/Low Amplitude Discontinuous and chaotic seismic (HADCh/LADCh) reflections	Rapid sediment accumulation, deformed internal structure, brittle to plastic deformation/laminar flow	Mass Transport deposits
F2 (a)			High Amplitude Continuous and Mounded (HACM) reflections	Reworking of sediments by along-slope bottom currents	Mounded Contourite deposits
F2 (b)			High Amplitude Continuous and Elongated (HACE) reflections		Plastered Contourite deposits
F3			High-Amplitude Continuous and Parallel (HACP) reflections with onlap terminations	Rapid sediment accumulation, turbulent flow	Turbidite deposits
F4			HACP and oblique reflections with toplap terminations	Sediment eroded due to relative sealevel fall	Progradation-degradation
F5			HACP reflection on top of a progradation-degradation facies	Sediment accumulation on the shelf/upper-slope related to high stand of sealevel	Progradation-aggradation

foreset and bottomset), separated by morphological breaks in the slope (points of maximum curvature) called rollover points (Pirmez et al., 1998). Clinotherm characterization was performed following the nomenclature and parameters proposed in Pellegrini et al. (2020) and was integrated with shelf-edge trajectory analysis that was originally proposed by Helland-Hansen and Martinsen (1996).

Isobath maps of two key reflections (Base Pliocene and ES5; Fig. 9A and B) were obtained from contour maps of the traveltimes to the seismic reflections, depth-converted using an inferred seismic velocity of 1500 m s<sup>-1</sup>, and interpolated using algorithms available in the package Halliburton-Landmark Decision Space® G1 Edition. Isopach maps display lines of equal thickness in the stratigraphic units measured perpendicular to the layer boundaries Base Pliocene – ES5 (Fig. 9C), ES5 – seabed reflection (Fig. 9D) and were automatically calculated from the

depth-converted contour maps. Whereas, the depocenter thickness map between Base Pliocene and seabed reflection was obtained with ESRI ArcGIS 10.5.1 by importing the ASCII points of the respective contour maps, that were interpolated into surface rasters using the kriging algorithm and processed using a cut/fill calculation (Fig. 9E).

### 3.3. Sub-bottom seismic reflection (SBS) profiles

SBS profiles were collected with a Teledyne Benthos CHIRP-III system, composed of a 16 hull-mounted transducer array, using a 2–20 kHz sweep-modulated bandwidth and 4 kW power per-channel, which allows a vertical resolution of about 50 cm and shallow penetration (< 100 m). Profiles were acquired during several surveys on board R/V Urania between 2005 and 2009. An additional SBS profile (RSM line in

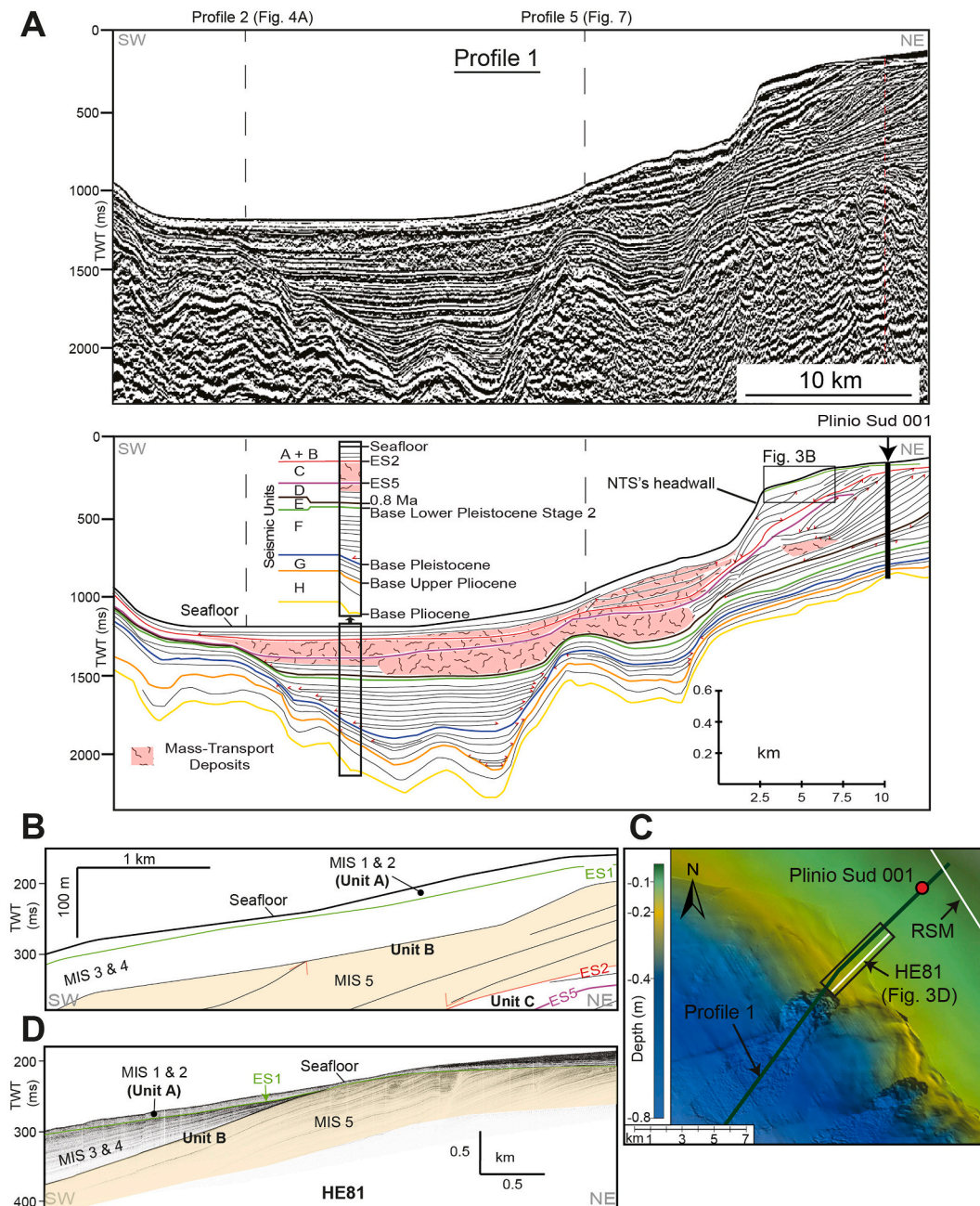


**Fig. 3.** A. Original seismic section and line drawing of MCS profile 1 crossing the borehole “Plinio Sud 001” (location in Fig. 2A). B. Enlargement of the prograding shelf-edge of MCS profile 1. C. Bathymetric map showing the location of B (black rectangle) and of SBS profile (white line) shown in D. D. Interpretation of SBS profile “HE81” showing the geometry of the seismic units A and B (Table 3) at the shelf edge. This profile was used to correlate the unconformity ES1 on MCS profile 1.

Fig. 7B), acquired with a similar system, was obtained from RINA Consulting S.p.A. All SBS profiles were post-processed with Geo Marine Survey Systems, Version 2.6. SBS profiles allowed to map ES1 (~30 kyr cal. BP; Kuhlmann et al., 2015) and ES2 (predating MIS 5e; Kuhlmann et al., 2015) that were correlated with MCS profiles (Figs. 3A, 4A and 5A). Isopach maps were obtained for stratigraphic units bounded by ES2 and ES1 (Fig. 9F), ES1 and the seabed reflection (Fig. 9G) with ESRI ArcGIS 10.5.1 and the same methodology described above. In addition, SBS profiles helped to characterize different surficial seismic facies, including contourite deposits and MTDs (Fig. 10).

### 3.4. Bathymetric data

The swath bathymetry data used in this work derive from several

surveys undertaken on board R/V Urania with different multibeam systems, including: 30 kHz Kongsberg-Simrad EM300, 50 kHz Reson Seabat® 8160, 70–100 kHz Kongsberg EM710, the latter used in 2007 during the MAKROS-CORSARO survey. The swath bathymetry data was merged with the 1/8 x 1/8 arc minutes resolution EMODnet compilation, where areas are not covered by actual soundings (EMODnet Bathymetry Consortium, 2016). From a 20-m-resolution swath bathymetry DTM (Fig. 11A), we obtained a slope gradient map (Fig. 11B), a slope aspect map (Fig. 11C) and a curvature map (Fig. 11D) using the tools provided in ESRI ArcGIS 10.5.1.

### 4. Results

The eastern side of the Gela Basin can be subdivided into three

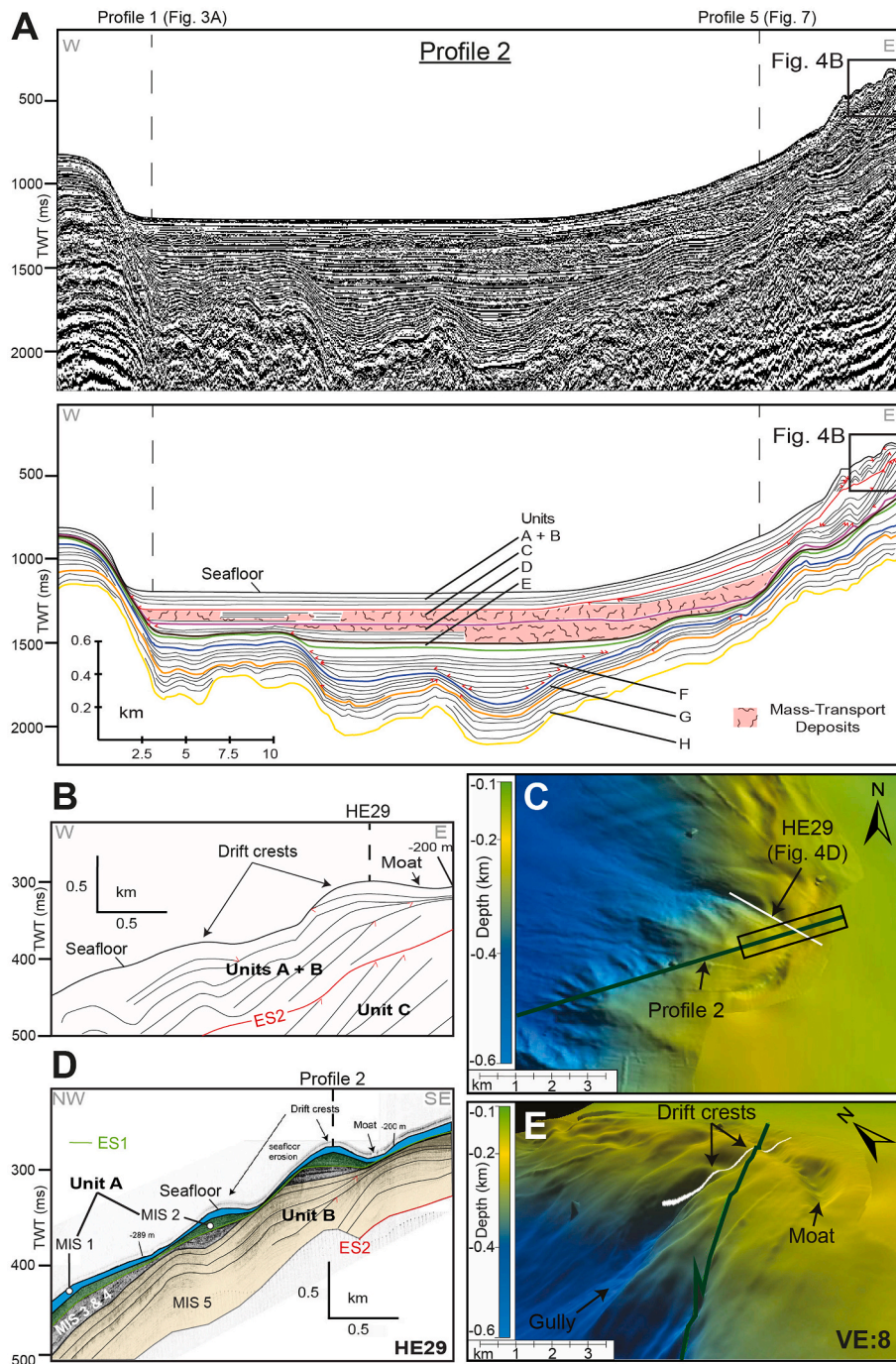


**Fig. 4.** A. Original seismic section and line drawing of MCS profile 2 highlighting the initiation of contourite deposits during the Upper Pliocene and their evolution through time. B. Enlargement of the prograding shelf-edge of MCS profile 2. C. Bathymetric map showing the location of B (black rectangle) and of SBS profile (white line) shown in D. D. Interpretation of SBS “HE29” highlighting the timing of contourrite growth in Sector 1. E. 3D bathymetric view of the area in C. See Fig. 3A and Table 3 for the description and interpretation of seismic units.

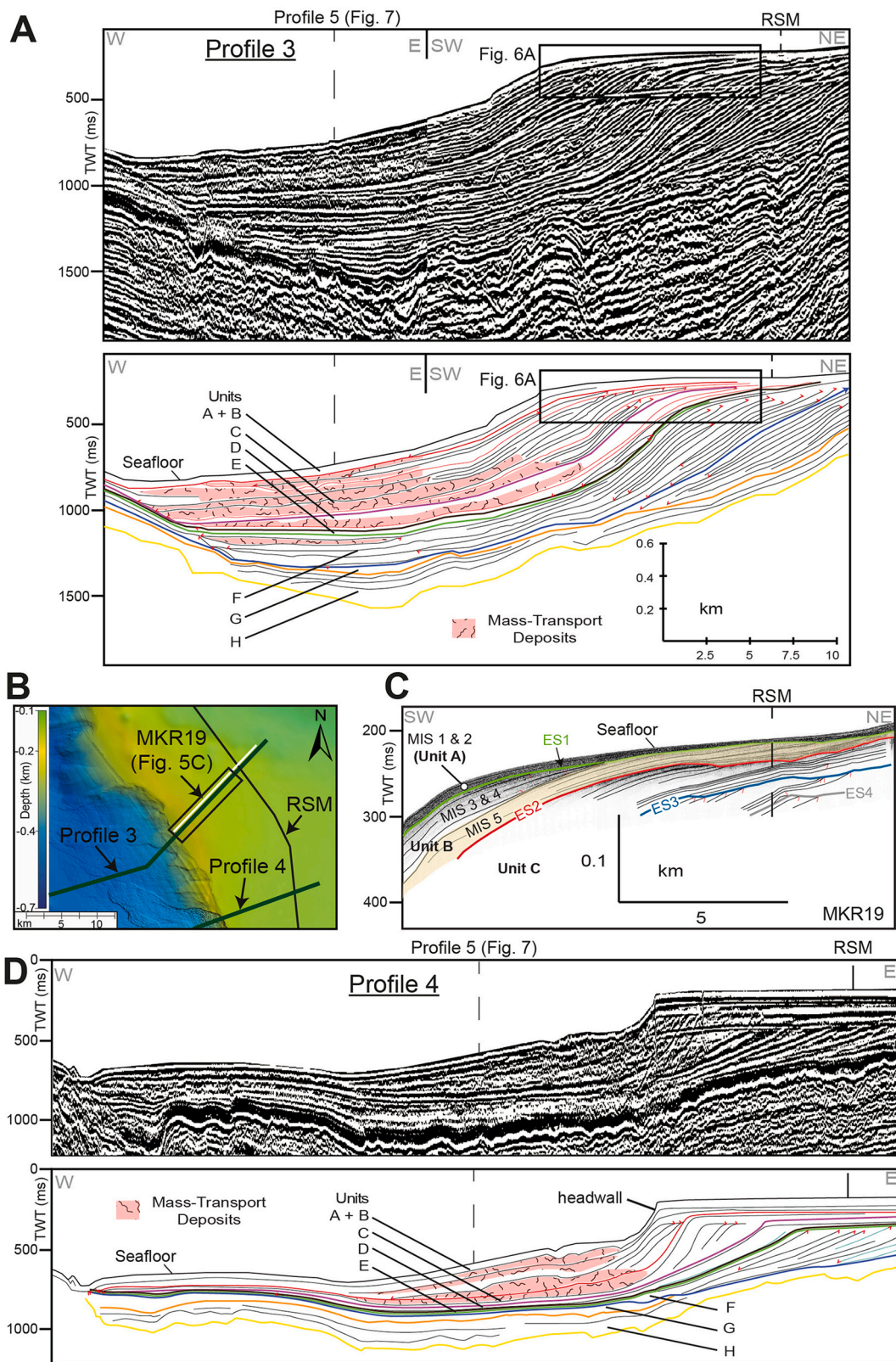


**Fig. 5.** A. Original seismic section and line drawing of MCS profile 3 showing the largest prograding set of the eastern Gela Basin. B. Bathymetric map showing the location of the enlarged area in Fig. 6A (black rectangle) and of SBS profile (white line) shown in C. C. Interpretation of SBS “MKR19” showing seismic units A, B and C (Table 3). D. Original seismic section and line drawing of MCS profile 4 showing oblique clinofolds during the Pliocene, top truncated strata and a net change in shelf aggradation after the MPT; same vertical and horizontal scales as in Fig. 5A. See Fig. 3A and Table 3 for the description and interpretation of the seismic units.

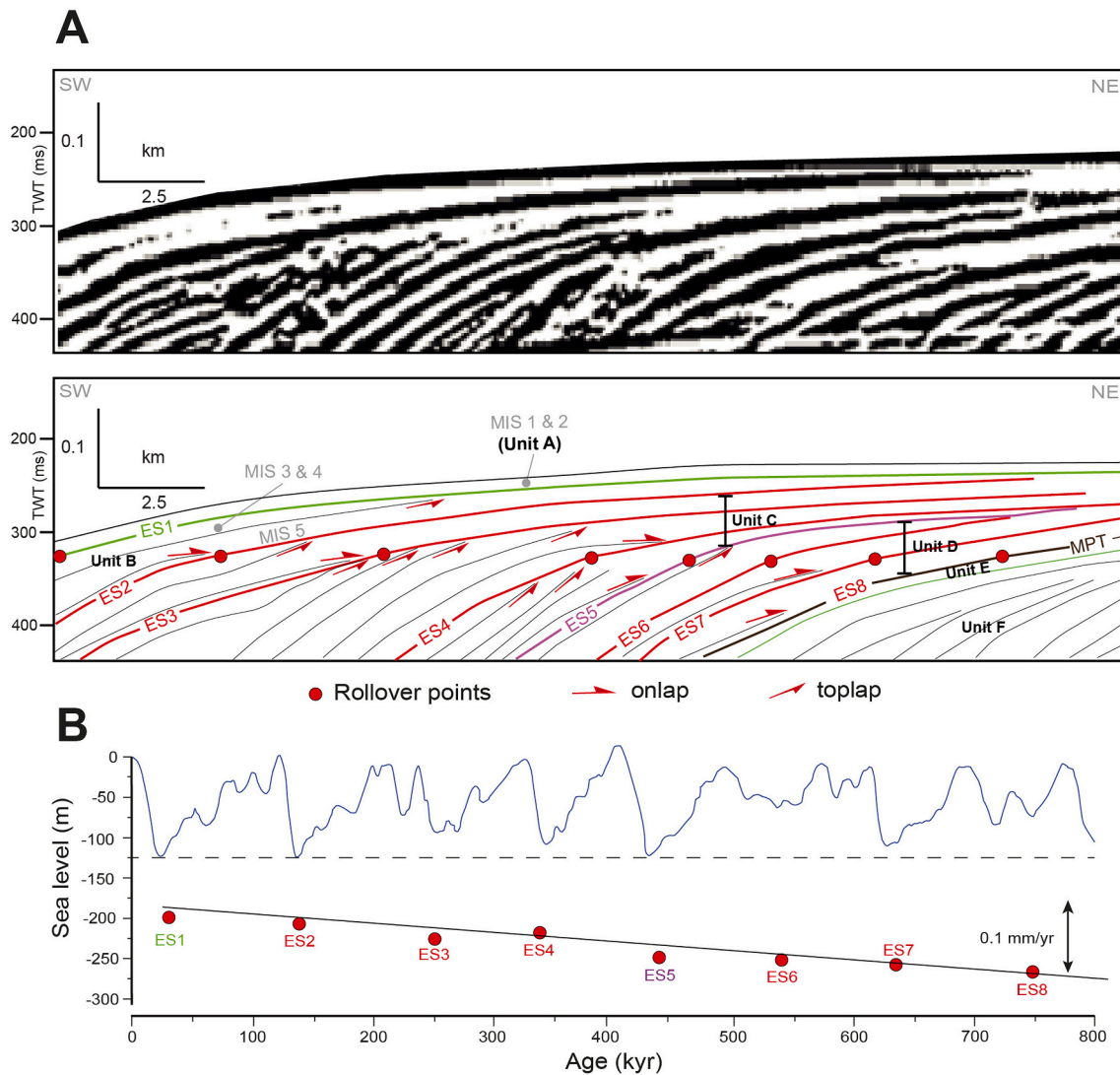


**Fig. 6.** A. Enlargement of the shelf-edge clinothems of MCS profile 3 of Fig. 5A bounded by the last eight erosional unconformities and highlighted by toplaps and onlaps (red arrows), showing a descending shelf-edge trajectory. B. Sea-level curve adapted from Spratt and Lisiecki (2006) with the corresponding rollover point for each erosional surface. Given the depth of rollover points (shoreline position) on the seismic profile, we estimated an average tectonic component of 0.1 mm/yr after the MPT, except for the last sea-level cycle when the tectonic vertical component is estimated at 2.5 mm/yr. (For interpretation of the references to colour in this figure legend, the reader is referred to the Web version of this article.)

sectors along a NW–SE direction, based on the Pliocene morphology (Fig. 9A). The map of the horizon corresponding to the Base of the Pliocene in fact shows two sub-basins up to 2.7 km deep located in Sector 1 (Fig. 9A), a headland at the shelf edge in Sector 2 and a bowl-shaped sub-basin in Sector 3 confined to the east by the Malta Plateau. The Pliocene–Quaternary sedimentary succession reached up to 2.4 km in thickness in Sector 1 and up to 1.2 km in Sector 3 (Fig. 9E) and can be subdivided in the units described in the following paragraphs.

#### 4.1. Seismostratigraphic units

A total of eight seismostratigraphic units from Lower Pliocene (Unit H) to MIS 1 (Unit A) were recognized between each key reflection in MCS and SBS profiles (Figs. 3–8 and 10), and were characterized by distinctive seismic facies (Table 2).

##### 4.1.1. Unit H (Base Pliocene – Upper Pliocene)

The H unit is characterized by a sheet drape external geometry at the base of the Pliocene–Quaternary succession (Fig. 7). From foresets to bottomsets, the unit increases in thickness reaching a maximum

thickness of 225 m in the bottomsets (Fig. 5A). In the along-strike profile, a decreasing in thickness is observed towards the south (Fig. 7). Overall, unit H shows a dominance of seismic facies F3 (Table 2) characterized by onlapping terminations in the two sub-basins of Sector 1 (Figs. 7A and 9A). Seismic facies F3 in the unit include both high and low amplitude reflections of interbedded layers (Table 2). The onlapping deposits of facies F3 reach a volume of almost 300 km<sup>3</sup> in Sector 1 for unit H (Figs. 3A and 4A and Table 4).

##### 4.1.2. Unit G (Upper Pliocene – base Pleistocene)

The G unit shows an overall sheet drape external geometry (Fig. 4A) and is characterized on the topsets by a sigmoid configuration (Fig. 5A). The unit has a maximum thickness of 250 m in the bottomsets (Fig. 3A) and is up to 220 m deep in the topsets (Fig. 5A). The G unit is mainly characterized by seismic facies F3 (Fig. 5A, Table 2).

##### 4.1.3. Unit F (Base Pleistocene – Lower Pleistocene)

The F unit shows an oblique tangential progradational configuration with a descending shelf-edge trajectory (Fig. 5A). The unit has a variation in thickness along the dip-oriented profile 1 from 100 m in the

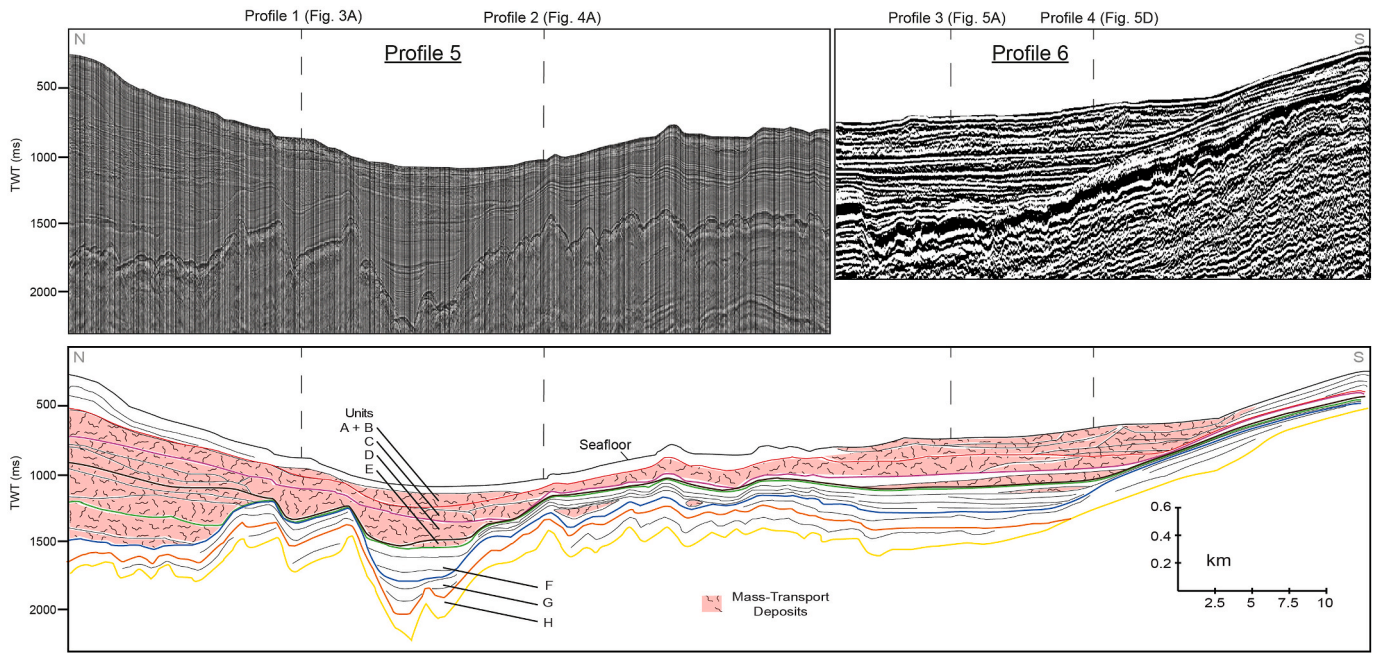


Fig. 7. A. Original seismic section and line drawing of MCS profiles 5 and 6 showing the along-strike variability (NW-SE direction) of the Pliocene-Pleistocene succession. See Fig. 2A for location.

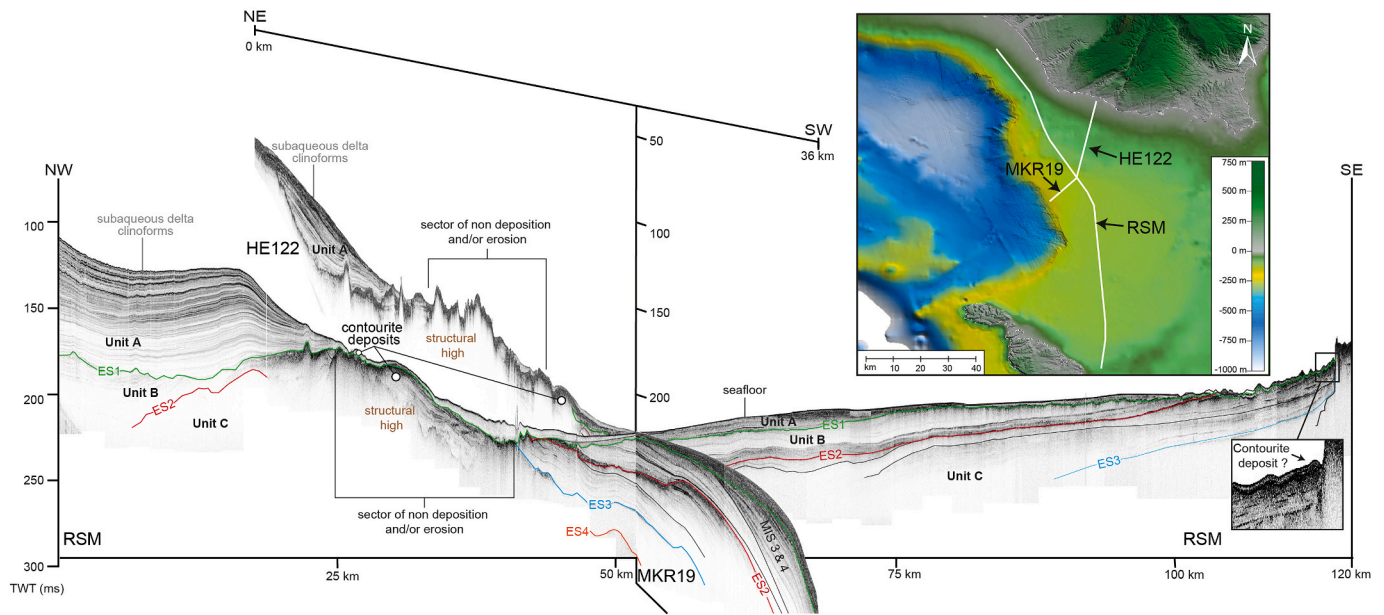


Fig. 8. SBS profile “RSM” which shows the younger clinothem (units A and B) crossed by SBS profiles “HE122” and “MKR19” (NE-SW direction) to highlight the changes in clinothem thickness along the shelf and the overall along-strike variability of the margin.

topsets to 350 m in the bottomsets (Figs. 3A and 4A). The topsets display also a lateral variability along the strike of the basin reaching up to 400 m thick towards the south (Fig. 5A). The unit is characterized by seismic facies F4 in the upper foresets (Fig. 5A) and by seismic facies F3 in the bottomsets (Fig. 3A, Table 2). Overall, onlapping deposits of seismic facies F3 have volumes of 4 km<sup>3</sup> in unit F (Table 4). In Sector 1, the unit is characterized by seismic facies F1 in the bottomsets, which corresponds to MTDs (Table 2) as thick as 200 m (Fig. 7).

#### 4.1.4. Unit E (Lower Pleistocene – MPT ~ 800 ka)

The E unit shows an overall sheet drape external geometry (e.g. Fig. 5D) and develops only in the north of the basin, where it reaches a

maximum thickness of 260 m in the foresets (Fig. 7). The unit is characterized by seismic facies F3 in the topsets-foresets (Fig. 3A) and seismic facies F1 in the bottomsets (Fig. 7, Table 2). The unit marks a change in the overall stacking pattern of the margin, with the appraisal in the foresets of seismic facies F2a, characterized by mounded reflections (Fig. 4A, Table 2).

#### 4.1.5. Unit D (MPT ~ 800 ka – ES5)

The D unit is represented by a complex sigmoid-oblique prograding reflection configuration with an ascending shelf-edge trajectory and reaches a maximum thickness of 350 m in the foresets (Fig. 3A). On the along-strike profile, the D unit shows a lateral variability in thickness

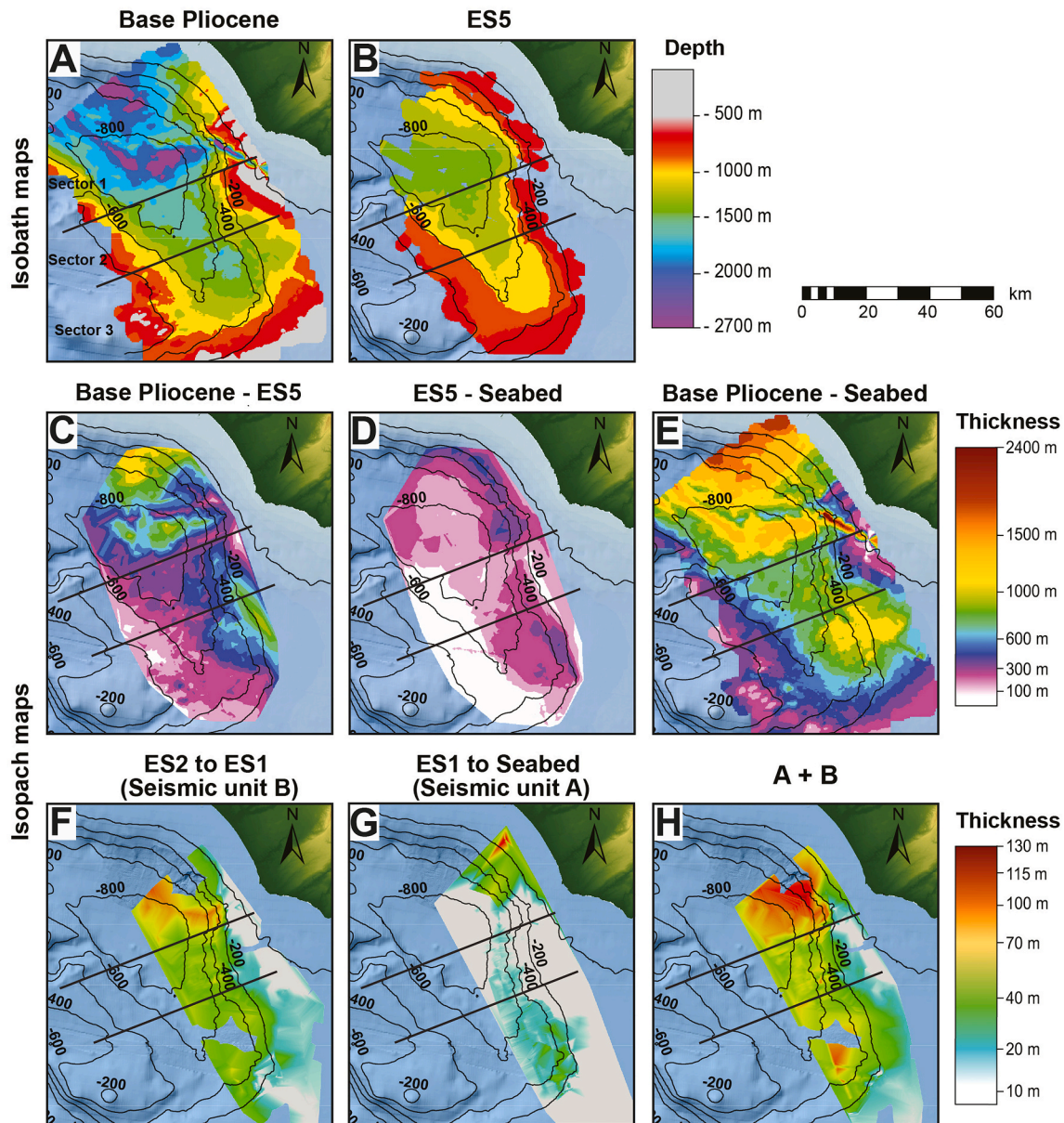


**Fig. 9.** Isobath maps (A and B) of key stratigraphic horizons and isopach maps (C, D, E, F, G) of significant stratigraphic units in the study area. C shows evidence of three sub-basins in Sector 1. D shows that sediment deposition was limited to the shelf edge during the corresponding time interval. E represents the overall Plio-Quaternary deposition showing maximum thickness in Sector 1. F and G are the sedimentation thickness between ES2 and ES1 and between ES1 and the seabed. H represents the sediment accumulation since ES2 until today (seismostratigraphic units A + B, Table 3) where it concentrated mainly on the slope of sectors 1 and 3.

with higher values in the north (Fig. 7). The unit is characterized by seismic facies F3 in the topsets (Fig. 5A), by seismic facies F2a in the foresets (Fig. 4A) and by seismic facies F3 and F1 in the bottomsets (Table 2, Figs. 3A, 4A and 5A, 5D and 7).

The isobath map of the ES5 reflection shows that the depocenters in the bottomsets of Sector 1 were partially filled during the Upper Pliocene and Lower Pleistocene (Fig. 9B), and depositional thickness reached up to 1.5 km in the two depocenters in the north and up to 1 km in the depocenter in the southeast (Fig. 9C). The shelf edge migrated < 5 km in Sector 1, < 1 km in Sector 2 and more than 20 km in Sector 3, before reaching the current position (Fig. 9B).

#### 4.1.6. Unit C (ES5 – ES2)

The C unit presents a stack of prograding clinoform sets that from north to south can be described as oblique (Fig. 4A), complex sigmoid-oblique with alternation of descending and ascending shelf-edge

trajectories (Fig. 5A), and oblique to complex sigmoid-oblique reflection configurations (Fig. 5D). The descending trajectories are highlighted by top truncated reflections at the outer shelf, whereas ascending trajectories are associated with minimum aggradation of the topsets (in the order of 10 ms; Figs. 5C and 8). The unit shows a maximum thickness of up to 385 m in the foresets (Fig. 5D, Table 3). In the basin, the unit is characterized both by seismic facies F1 (Figs. 3A, 4A and 5A, 5D and 7) and F3 (Fig. 5A and D, Table 2). The thickness between ES5 and the seabed is up to 450 m in Sector 1 and 400 m in Sector 3 (Fig. 9D).

#### 4.1.7. Unit B (ES2 – ES1 ~ 30 ka)

The B unit shows a complex sigmoid-oblique reflection configuration (Fig. 3A) and an increase in thickness in the lower foresets, where it reaches more than 200 m (Figs. 3A and 7B). The B unit is characterized by seismic facies F4 in the topsets (Fig. 3D) and seismic facies F3 in the bottomsets passing laterally to seismic facies F1 at the base of the slope

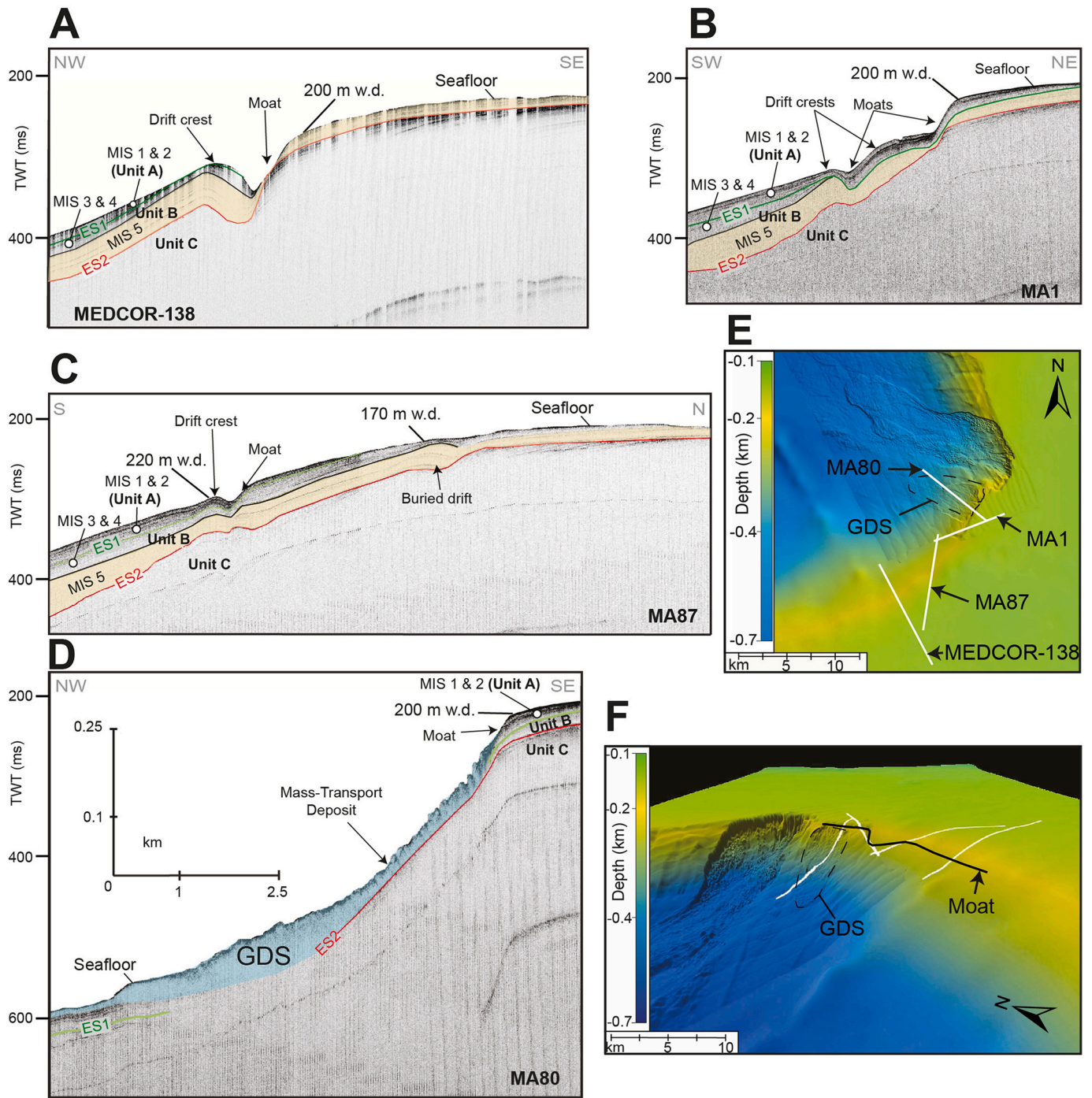


**Fig. 10.** A. SBS profile “MEDCOR-138” showing the internal structures of the most prominent contourite deposit in the upper slope of Sector 3. Seismic units A and B show that the deposition of the drift crests occurred mainly during MIS 5 (see also Table 3). B. SBS profile “MA1” showing the continuity of the contourite deposits along the shelf edge and upper slope. C. SBS “MA87” showing the presence of a buried drift developed on top of ES2. D. SBS “MA80” shows a moat and the Gela Drift Slide (GDS) gliding on top of the erosional surface ES2. E. Bathymetric map with location of the seismic profiles shown in A, B, C and D. F. 3D bathymetric view showing the GDS deposit located downslope the failed drift crests. Horizontal and vertical scales of SBS profiles are given in Fig. 10D.

(Figs. 3A, 5A and 5D, Table 2).

From ES2 to ES1, sedimentation is limited in the foresets and bottomsets with a deposition thickness up to 100 m (Fig. 9G). MIS 5 deposits are 150 m thick in the topsets, however SBS profiles penetrated the deposit until the rollover point between the foresets and topsets and ES2 is not visible.

4.1.8. Unit A (ES1 ~ 30 ka – present)

The A unit shows an overall sheet drape external geometry in the

topsets (Figs. 3D and 5C) with a sigmoidal configuration (Fig. 8) which, along with the continuous coastal seismic reflections, suggest the presence of a mud belt up to 50 m thick (Fig. 8). On the dip-oriented profile, the A unit increases in thickness towards the lower foresets reaching up to 40 m in the south (Fig. 10A). Here, the A unit is characterized by the occurrence of moats oriented along the contours (Fig. 10). The unit is characterized by seismic facies F3 in the topsets (Fig. 8) and the lower foresets (Fig. 10D) and by seismic facies F2b in the upper foresets (Figs. 4 and 10). This unit exhibits two depocenters, a 50 m thick depocenter

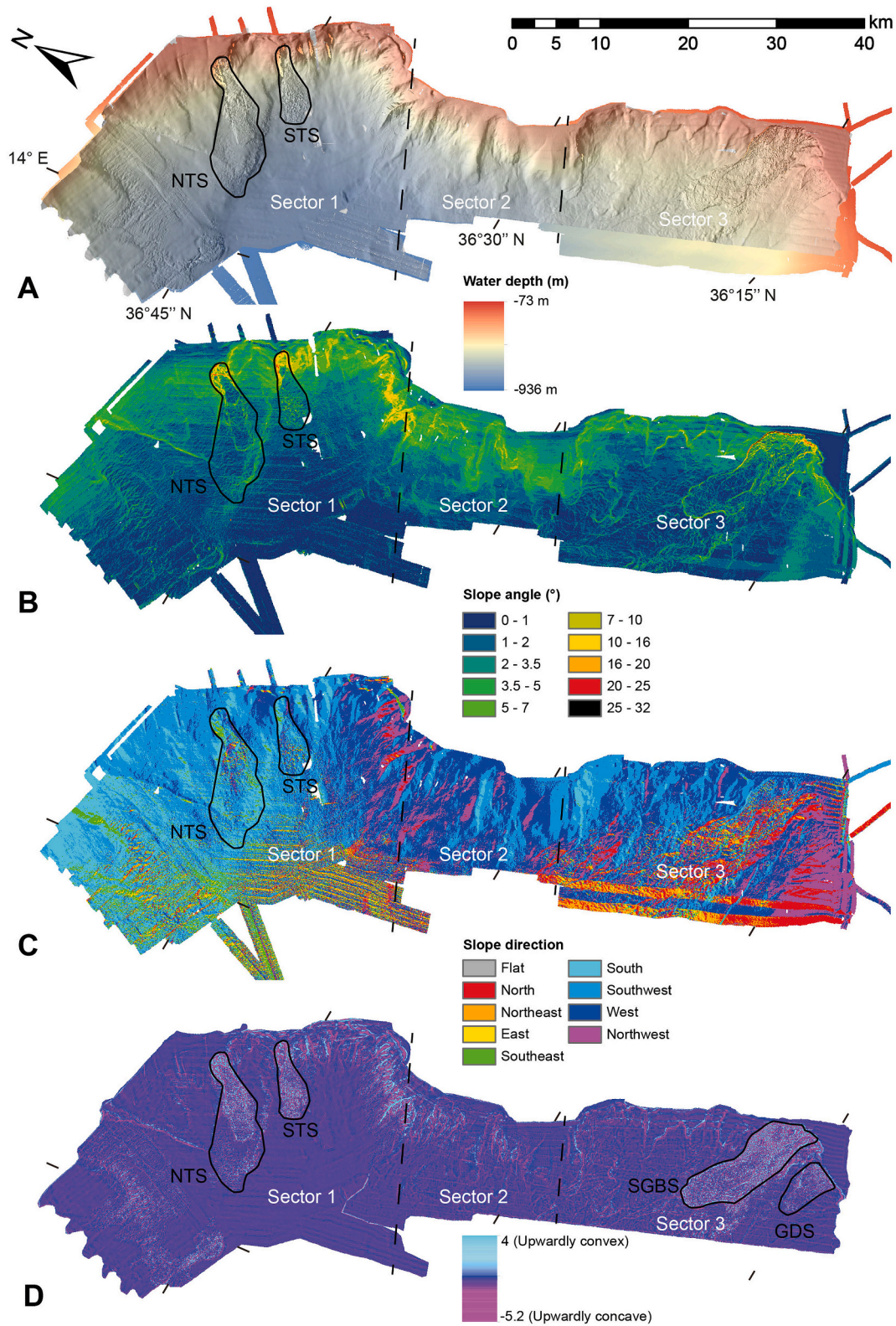


**Fig. 11.** A. Shaded-relief map of the 25-m-resolution DTM of the eastern margin of the Gela Basin subdivided in three sectors and highlighting the mass-transport deposits (MTDs) described in previous studies (Northern Twin Slide–NTS and Southern Twin Slide–STS). B. Slope gradient map showing an average gradient of 2.1° and up to 32° at the shelf edge of sectors 1 and 3. C. Aspect map showing a southern direction in Sector 1 and an N–NW direction in sectors 2 and 3. D. Curvature map revealing hummocky surfaces corresponding to the MTDs discovered by this study (Southern Gela Basin Slide–SGBS and Gela Drift Slide–GDS).

**Table 3**

Details of seismic units A to H identified in the seismic profiles and correlated with borehole and sediment core data. For the descriptions of seismic facies refer to Table 2.

Seismic units	Lower boundary	Upper boundary	Age		Thickness range (m)	Seismic facies	Description	Interpretation	
A	ES1	Seafloor	MIS 1	MIS 2	0–119	HACP and HADCh	Sheet drape	Low sedimentation since last sea-level lowstand	
B	ES2	ES1	MIS 3	MIS 4	MIS 5	50–250	HACP and HADCh	Complex sigmoid-oblique configuration with toplap terminations and chaotic reflections in the basin	Changes in relative sea level and presence of MTDs
C	ES5	ES2	Middle Pleistocene - Stage 2		0–385	HACP and HADCh	Complex sigmoid-oblique configuration with alternation of descending and ascending trajectories along with chaotic reflections in the basin	Changes in relative sea level and presence of MTDs	
D	MPT	ES5	Middle Pleistocene - Stage 1		10–350	HACP, HACM and HADCh	Complex sigmoid-oblique configuration with ascending trajectories and onlap terminations along with chaotic reflections in the basin	Growth of contourite deposits and presence of MTDs	
E	Lower Pleistocene	MPT	Lower Pleistocene - Stage 2		0–260	HACP, LADCh and HACM	Sheet drape and mounded reflections along with chaotic reflections in the basin	Initiation of contourite deposits and presence of MTDs	
F	Base Pleistocene	Lower Pleistocene	Lower Pleistocene - Stage 1		0–400	HACP and LADCh	Complex sigmoidal to oblique tangential configuration with descending trajectories along with chaotic reflections in the basin	Relative sea-level fall and presence of MTDs	
G	Upper Pliocene	Base Pleistocene	Upper Pliocene		0–250	HACP	Sheet drape and sigmoid configuration	End of the Zanclean flood and initiation of the progradation	
H	Base Pliocene	Upper Pliocene	Lower Pliocene		0–225	HACP and HAD	Sheet drape and onlap terminations	Start of sedimentation after the Zanclean flood	

located in the topsets in Sector 1, and a 40 m thick depocenter in the foresets in Sector 3 (Fig. 9G). Inside unit A, sediments deposited after ES2 mostly occur along the slope of sectors 1 and 3 (Fig. 9H).

#### 4.2. Seafloor morphology and seismic facies

The high-resolution bathymetry shows a shelf edge at 200 m w.d. and a basin as deep as 936 m w.d. in Sector 1 (Fig. 11A). The average slope gradient is 2.1° with maximum local values of 32° at the headwall

scars of the Twin Slides (NTS and STS in Fig. 11A) and in the south of Sector 3 (Fig. 11B). The slope angle is 1–10° in sectors 2 and 3 (Fig. 11B), and both sectors display changes in the slope direction from SSW to NNW (Fig. 11C), forming a curvature of the margin and creating large amphitheatre-like morphologies, characterized by upwardly convex and concave structures (Fig. 11D).

The short-distance changes in slope direction and gradient define the contourite moats located in 200 m w.d. in Sector 1 (Fig. 4C and E) and in Sector 3 (Fig. 10F). The moats are 3.5 long and 40 m deep (Fig. 4D) in

**Table 4**

MTDs and turbidite deposits observed in the seismic profiles available in the study area, accompanied by their inferred recurrence times, dimensions, source directions, location along the margin sectors and likely controlling factors.

Time	Seismic Unit	Type	Recurrence (Myr)	Area (km <sup>2</sup> )	Thickness (km)	Volume (km <sup>3</sup> )	Source	Sector	Name	Controlling factors
Upper Pleistocene-Holocene	A + B	MTD	0.1	15.5	0.037	0.5735	NE	1	NTS	Eustasy
		MTD	0.1	14.4	0.025	0.36	NE	1	STS	Eustasy
		MTD	0.1	8	0.05	0.4	SE	3	GDS	Oceanographic
		MTD	0.1	350	0.05	17.5	NE	1	FS	Oceanographic
		MTD	0.1	100	0.05	5	NE	1		Oceanographic
		MTD	0.1	120	0.05	6	NE	1		Oceanographic
		MTD	0.1	580	0.04	20	SE	3		Eustasy
Middle Pleistocene-Stage 2	C	MTD	0.1	580	0.04	17	SE	3		Eustasy
		MTD	0.35	800	0.12	96	N	1		Tectonic
		MTD	0.1	48	0.05	2.4	SE	3		Eustasy
		MTD	0.1	26	0.05	1.3	SE	3		Eustasy
		MTD	0.1	47	0.05	2.35	SE	3		Eustasy
		MTD	0.1	25	0.05	1.25	SE	3		Eustasy
Middle Pleistocene-Stage 1	D	MTD	0.1	760	0.12	91	SE	2/3		Eustasy
		MTD	0.3	375	0.12	45	NE	1		Oceanographic
		MTD	0.1	286	0.04	11.44	SE	3		Eustasy
		MTD	0.1	550	0.066	30	N	1		Tectonic
		MTD	0.1	550	0.066	35	N	1		Tectonic
Lower Pleistocene-Stage 2	E	MTD	0.1	550	0.066	40	N	1		Tectonic
		MTD	0.6	1032	0.1	100	N	1		Tectonic
		MTD	0.6	1032	0.1	120	N	1		Tectonic
		MTD	0.6	1032	0.1	80	N	1		Tectonic
Lower Pleistocene-Stage 1	F	MTD	1.8	119	0.04	4.76	E	1		Oceanographic
		MTD	0.5	1032	0.1	110	N	1		Tectonic
		MTD	0.5	1032	0.1	90	N	1		Tectonic
Upper Pliocene	G	Turbidite	1	411	0.34	139.74	E	1		
		Turbidite	1.7	1740	0.17	295.8	NE	1		

Sector 1 and 9 km long and 70 m deep (Fig. 10A) in Sector 3. Contourite deposits display mounded reflections in SBS profiles that highlight the internal structures of the drift crests in Sector 1 (Fig. 4B and D) and Sector 3 (Fig. 10). Drift crests that developed on top of ES2 are mainly composed of sediments deposited during MIS 5 with a 60 m thick accumulation in Sector 3 (Fig. 10A).

In Sector 1 the Twin Slides deposits show a southern slope direction while areas in the south of Sector 3 show a northern and eastern slope direction, which contrast with the main NW slope direction of sectors 2 and 3 (Fig. 11C). Upward convex or concave features are observed downslope steep headwalls and are thus interpreted as mass-transport deposits (MTDs) and named South Gela Basin Slide (SGBS) and Gela Drift Slide (GDS; Figs. 10D and 11D). Their headwall scars reach lengths of 12.1 km and 3.6 km, respectively. The GDS in particular is characterized by transparent to chaotic seismic facies and reaches a maximum thickness of 50 m with an estimated volume of 0.41 km<sup>3</sup> (Fig. 10D and Table 4).

## 5. Discussion

### 5.1. The Pliocene–Quaternary stratigraphic architecture of the Gela Basin

The Pliocene–Quaternary stratigraphic architecture of the Gela Basin

records two main phases of margin outbuilding characterized by changes in depositional patterns as well as a drastic change in sediment accumulation rates.

#### 5.1.1. Progradational phase (Pliocene – MPT)

The Lower Pliocene was characterized by the deposition of parallel strata draping the uneven pre-existing morphology and marking the inundation of the Mediterranean Sea from the Atlantic Ocean after the opening of the Gibraltar Strait (Zanclean flood in Table 3; Garcia-Castellanos et al., 2009). The inherited uneven morphology, characterized by two deep sub-basins, determined the position of the Plio-Quaternary depocenters. Above sub-parallel strata, a 300-m-thick sediment wedge deposited during the Upper Pliocene recording a basinward migration of the shelf edge of ca. 10 km in Sector 3 (Fig. 5A), and with the concomitant infilling of the structural sub-basins in sectors 1 and 3 by onlapping strata ascribed to turbidite deposits by Ghielmi et al. (2012) (Figs. 3A, 7 and 13). In the Pleistocene, progradation extended to the south with the emplacement of oblique shelf-edge clinothems (Fig. 5D). The top truncated strata of these clinothems coupled with the flat to slightly descending shelf-edge trajectory may reflect the Lower Pleistocene uplift of the Malta Plateau documented by Gardiner et al. (1995) (Fig. 12). From Pliocene to MPT, the sediment wedge increased in thickness by 150 m/Myr, with the main depocenters located in Sector 1

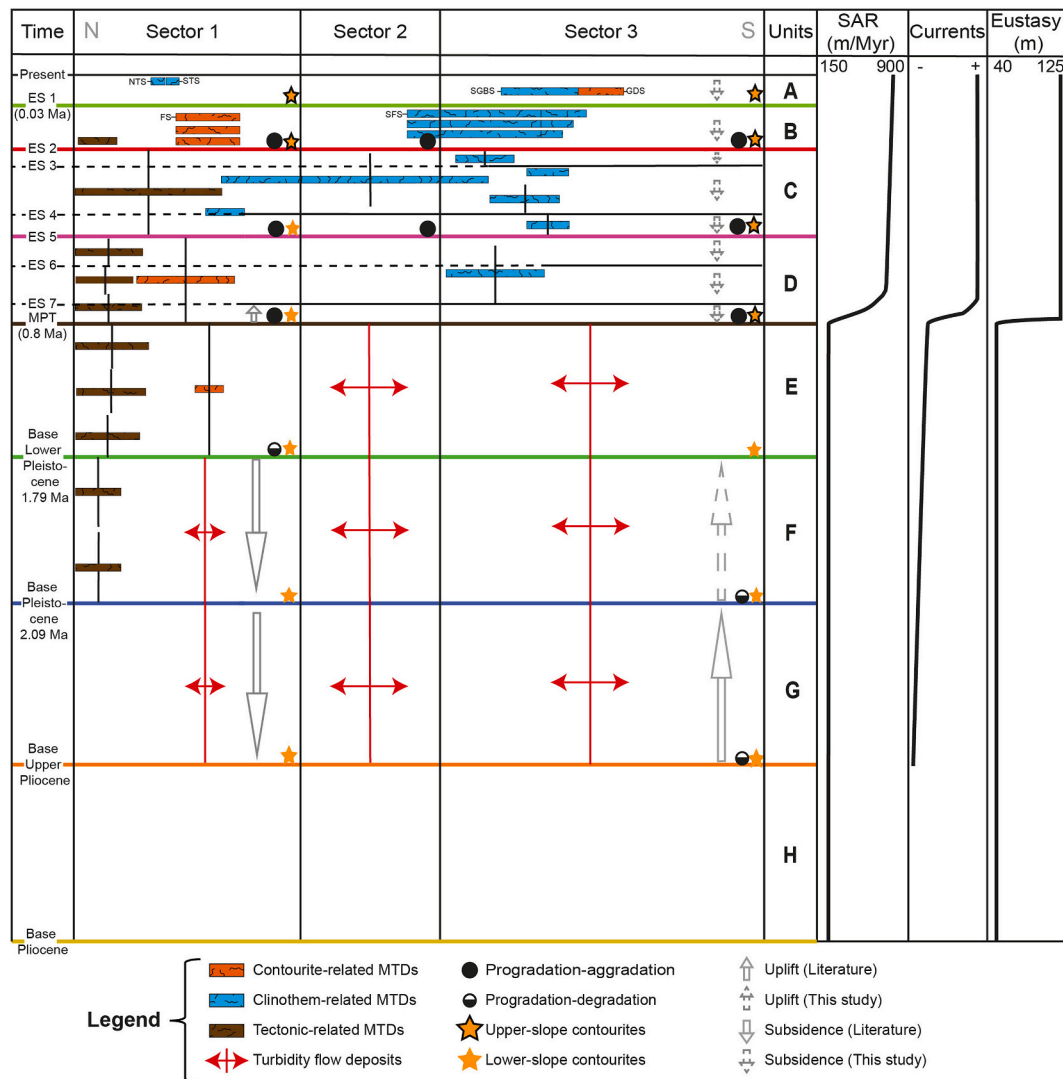
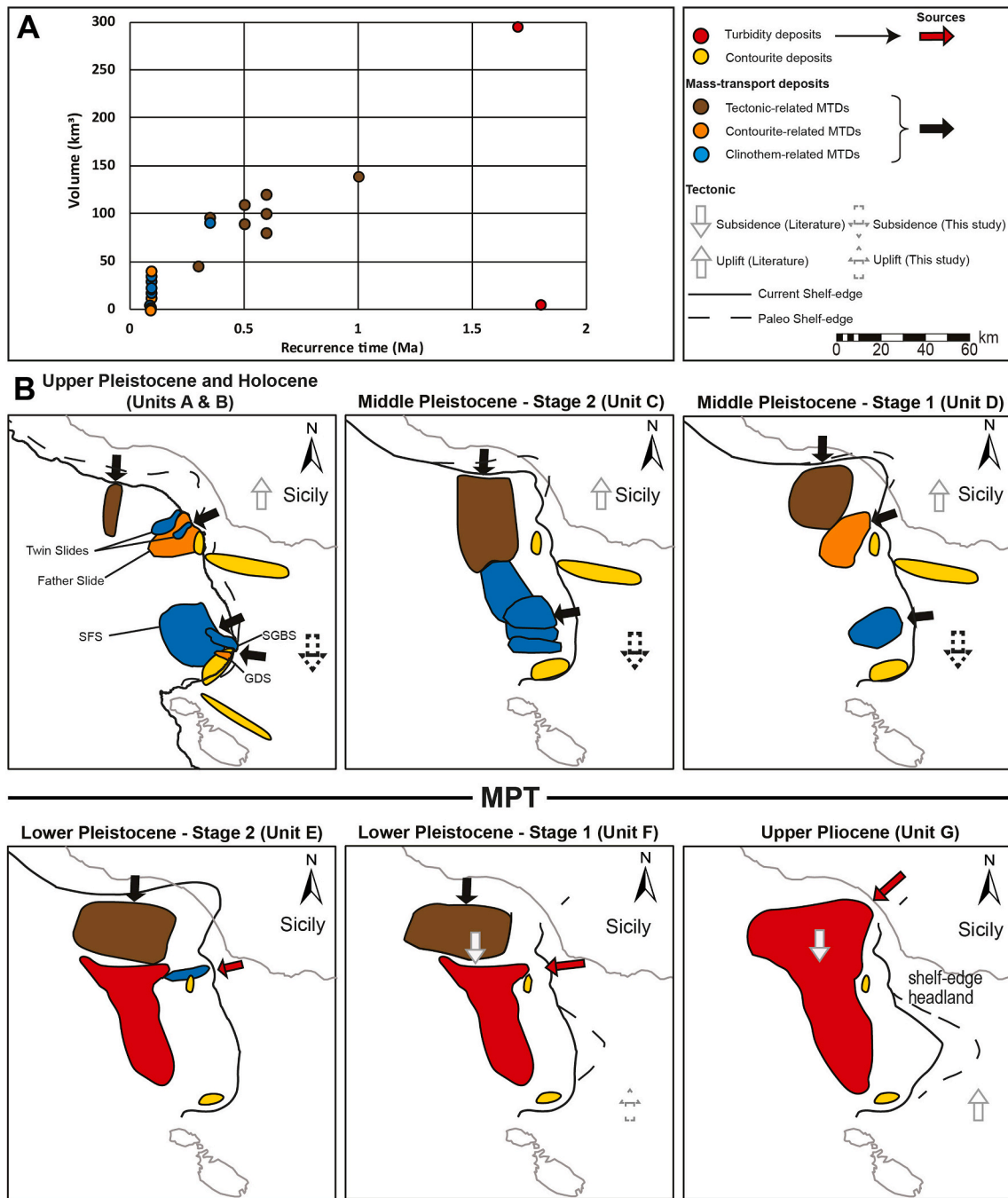


Fig. 12. N–S oriented chronostratigraphic cross-section summarizing the evolution of the eastern Gela Basin since the Pliocene. The temporal distribution of the deposits is schematic. SAR: sediment accumulation rate.



**Fig. 13.** A. Recurrence time plotted against reconstructed volumes of mass-transport deposits (MTDs) and turbidite deposits mapped in the eastern Gela Basin since the Pliocene (see also Table 4). B. Time sketch of the eastern Gela shelf-edge margin growth (black lines) for the Pliocene to Quaternary along with the distribution of sedimentary bodies and MTDs.

and in the east of Sector 3 (Fig. 12).

5.1.2. Progradational-aggradational (MPT – present)

The MPT horizon (Table 3) coincided with a general reorganization of the margin growth and of the stratigraphic architecture (Fig. 12). The margin outbuilding evolved from a progradational to a progradational with strongly aggradational motif (e.g. Fig. 5A), suggesting an overall increase in accommodation on the continental shelf accompanied by an increased sediment flux in all three sectors of the margin (Fig. 13). Like other continental margins (Ercilla et al., 1994; Fatoke and Bhattacharya, 2010; Gong et al., 2016), the deposition of thick sedimentary bodies after the MPT was accompanied by the increased occurrence of MTDs

and the Gela Basin recorded the destabilization of the entire eastern slope with the emplacement of several submarine landslides (Figs. 10, 11D and 15B).

The sedimentation rate of the progradation-aggradation phase reached 900 m/Myr, likely contributing to increased sediment load and causing subsidence of the shelf. The subsidence was previously documented by Gardiner et al. (1993), however they attributed the sinking to normal faulting. From the comparison with the underlying Pliocene–Lower Pleistocene progradational phase, a six-fold increase in the rate of margin outbuilding occurred after the MPT. This finding has implications for the geological time recorded by clino-stratified successions, and suggests that the physical scale of the lithosomes recorded

in the stratigraphic succession is unrelated to the time elapsed during their deposition as observed on other margins (Miall, 2016; Pellegrini et al., 2017a; Smith et al., 2015).

### 5.1.3. Slope instability and different types of MTDs

We analysed the morphology of the accumulation areas of MTDs, the orientation and shape of their headwall scars and their volumes to infer which predisposing factor (tectonics, shelf progradation, bottom currents) was predominant in their mobilization during the Pliocene and Pleistocene (Table 4). In the north (Sector 1), tectonic vertical movements were prevailing until the MPT, likely reflecting the proximity of the Maghrebian fold-and-thrust belt (Fig. 1) and the Messinian deformation that initiated the general uplift and exhumation of the accretionary wedge while the Hyblean Plateau locally forced uplift at the orogenic front (Henriquet et al., 2020). Transtensional movements concentrated during Late Miocene to Pliocene, resulting in a N–S extension in the Pantelleria Graben (PG in Fig. 1; Martinelli et al., 2019), with minimum effects in the study area. MTDs linked to extensional tectonics have distinct signatures, including blocks, debris-flow deposits and chaotic volumes from turbidites (Alves and Gamboa, 2019). The MTDs emplaced in the Upper Pliocene and Lower Pleistocene in the study area have prominent headwall scars, blocky to chaotic seismic facies and are sourced from the north (Table 4, Figs. 12 and 13), similar to the Gela Slide, which was triggered by the uplift of the Gela Nappe (Trincardi and Argnani, 1990). These tectonic-related MTDs are in the range 30–120 km<sup>3</sup> and have been deposited roughly every 400 kyr (Table 4, Fig. 13A).

After the MPT, only minor local subsidence on the Malta Plateau (Gardiner et al., 1993) and regional uplift in the Hyblean Plateau (Ghielmi et al., 2012) occurred, with no significant impact on sediment supply. In sectors 2 and 3, contourite-related MTDs formed downslope of contourite deposits involving volumes from 0.4 km<sup>3</sup> to 45 km<sup>3</sup> with a recurrence possibly influenced by the 100 kyr glacial/interglacial timescale climate variability (Figs. 10D, 12 and 13, Table 4).

In sectors 1 and 3, the high sediment accumulation rate at the shelf edge caused an increase of the slope gradient, which contributed to the margin instability, as previously suggested by Minisini and Trincardi (2009). Clinothem-related MTDs were thus emplaced where the margin had the highest sediment input, possibly related to the occurrence of river networks as suggested by Kuhlmann et al. (2015), coupled with the activity of persistent bottom currents (Fig. 8). The clinothem-related MTDs have volumes averaging at about 23 km<sup>3</sup> and reflect an eustatic control with a pacing similar to the contourite-related MTDs (Table 4, Figs. 12 and 13).

## 5.2. Contourite deposits as key markers of stratigraphic architecture

### 5.2.1. Onset of contourite deposits

Despite having been described in previous studies (Marani et al., 1993; Martorelli et al., 2001; Micallef et al., 2013; Verdicchio and Trincardi, 2008a,b), the timing of the onset of contourite deposits in the Strait of Sicily remains elusive. Our data show that the Upper Pliocene horizon marks the onset of contourite deposition on the lower slope of sectors 1 and 3 of GB, where mounded and plastered drifts (*sensu* Stow and Faugères, 2008, Table 2) developed, respectively (Figs. 12 and 13). The mounded drifts onset at the toe of the slope and progressively migrated upslope (Figs. 4B and 12). We ascribe the presence of thicker contourite drifts in Sector 1 (Fig. 4B and D) to the activity of a paleo bottom current interacting with the uneven topography inherited since the base of the Pliocene (see the structural high in Figs. 8, 9A and 9E). Integrated sedimentological and oceanographic analyses have recently shown that such mounded drifts typically characterize slope sectors where deceleration of bottom current promotes deposition, whereas plastered drifts tend to form in sediment-starved margin sectors (Miramontes et al., 2018). In our case, the presence of the structural high with a pronounced shelf-edge bulge (Fig. 8) led to the deposition of

contourite deposits on its up- and down-current sides (Fig. 13) as discussed elsewhere by Falcini et al. (2016) and Rovere et al. (2019).

### 5.2.2. Evolution of contourite deposits

After the MPT, the accelerated growth of contourite deposits along the whole margin (Figs. 12 and 13) implies the enhanced activity of near-seafloor water masses along the slope similar to the modern LIW, as suggested in other basins of the Mediterranean Sea (Amelio and Martorelli, 2008; Miramontes et al., 2016; Pellegrini et al., 2016). A bottom current should have a speed range > 10–12 cm s<sup>-1</sup> and < 20 cm s<sup>-1</sup> to initiate erosion and subsequent deposition of mounded sediment drifts in fine-grained sediments (e.g. McCave and Hall, 2006; Stow et al., 2009). The LIW circulates in the Strait of Sicily with a velocity of 13 cm s<sup>-1</sup> (Lermusiaux and Robinson, 2001), but may undergo intensity fluctuations, as observed in the Corsica Channel, possibly influenced by climatic changes on Milankovitch timescales (Toucanne et al., 2012).

### 5.2.3. Bottom currents strength and sea level variations

In an attempt to define when and where contourite deposits grow in relation to sea-level variations, Verdicchio and Trincardi (2008a) inferred an increased strength of the LIW during interglacials in the Central Mediterranean, while Miramontes et al. (2016) inferred faster bottom currents during cold intervals in the Corsica Channel. Our SBS profiles indeed show that the most recent growth of contourite deposits occurred during late MIS 2 and MIS 5 (Figs. 4D, 8 and 10) in the Gela Basin, supporting the action of bottom currents during both late glacial and interglacial periods, as envisaged in other contexts (e.g. Brackenridge et al., 2011).

High sediment accumulation rates (200 cm kyr<sup>-1</sup>) in the prograding clinothems during MIS 5 in Sector 1 were observed in previous studies (Kuhlmann et al., 2015). Our data show a thickness decrease of MIS 5 deposits proceeding southward from Sector 1 to Sector 2 (Fig. 8). However, MIS 5 deposits increase their thickness in Sector 3 with a sediment accumulation rate at 100 cm kyr<sup>-1</sup>, where contourite drifts formed (Fig. 10). This evidence seems to indicate that sediments by-passed Sector 2 along a seaward bulge of the shelf edge (headland) and accumulated downcurrent in Sector 3, under the action of the LIW (Fig. 1).

### 5.2.4. Contourites and erosional surfaces as predisposing factors to margin instability

In the Gela Basin, the growth of contourite deposits is concomitant with an increase in the occurrence and decrease in the size of MTDs in the basin (Figs. 12 and 13). This finding suggests a causal relation between the development of contourites and the emplacement of MTDs. Since the growth of contourite deposits on the slope, large sectors of the slope destabilized, involving in some cases the entire stratigraphic succession (Fig. 12) and promoting an increase in the number of MTDs, with volumes ranging from 0.5 to 40 km<sup>3</sup>, named contourite-related MTDs (Fig. 13A). In Sector 3, the Gela Drift Slide (GDS) affected a large extent of a contourite drift with the Erosional Surface ES2 at its base, possibly acting as a glide plane (Fig. 10D). Previous studies suggested that weak layers such as intercalated volcanoclastic layers (Kuhlmann et al., 2017) create a basal change in mechanical properties which, together with increased pore pressure induced by rapid deposition (Urlaub et al., 2013) and higher slope gradient (Miramontes et al., 2018) as in the case of contourites, may favour the initiation of margin destabilization. In the case of the GDS, we suggest that the ES2 might have acted as a weak layer, due to a change in grain size, as reflected by the change in acoustic impedance in the seismic profiles (Fig. 10D). Contourite deposits are comprised of fine-grained sediments in the Gela Basin, alike in the Mediterranean Sea due to the average limited availability of coarser grained deposits on the shelf (Mulder et al., 2008), and differ in grain size from sediments deposited during lowstands. This mechanism has been suggested also for the Brazilian margin (Alves, 2010) and is supported by the evidence that, since the MPT, MTDs in the Gela Basin

consistently develop atop of regional lowstand unconformities (Fig. 5A).

5.3. Climate as main driver of clinothem architecture and margin instability after the MPT

We analysed reflection terminations to define sequence boundaries and related depositional sequences reconstructing timing of sediment delivery in the Gela Basin. There commonly are, however, a variety of erosional surfaces of different duration and lateral extents observable on shelves that can be interpreted potentially as sequence boundaries (e.g.

Pellegrini et al., 2017b; Madof et al., 2017, 2019). Sequence-stratigraphic models refer to the formation of a sequence boundary either at the beginning (e.g. Posamentier et al., 1992) or the end of the eustatic fall (e.g. Hunt and Tucker, 1992). Following the classic definition of sequence boundary by Mitchum et al. (1977), we were able to distinguish sequence boundaries from other erosional surfaces by differentiating the types and extents of their toplaps and onlaps at the shelf and on the slope, respectively (Figs. 5A, 6 and 14). We analysed the character of these surfaces along a ca. 100 km stretch of the Gela Basin (Figs. 5A, 6 and 14) and observed: i) the flat to slightly

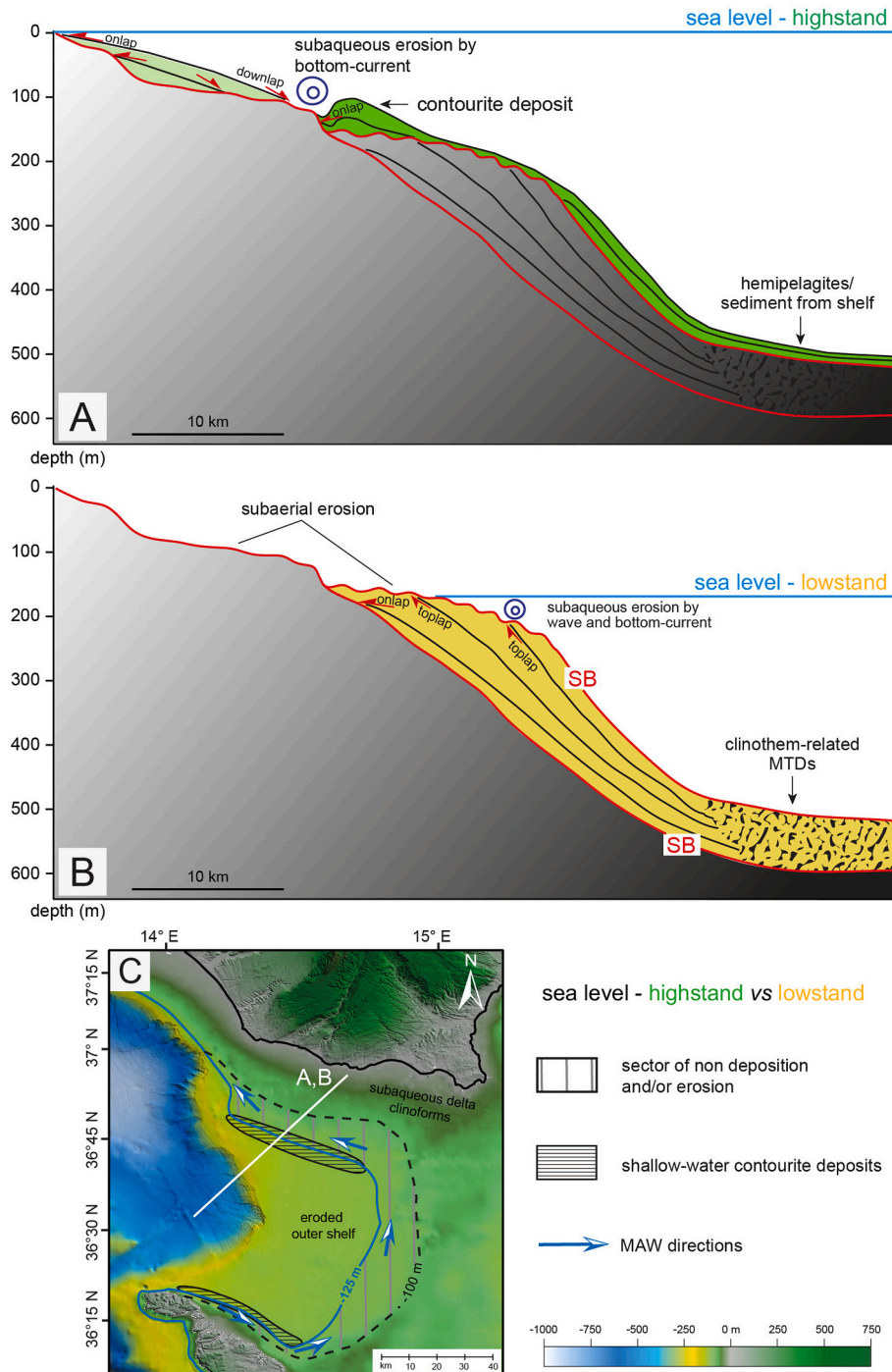


Fig. 14. Along-dip shelf stratigraphic reconstructions illustrating the changes in sediment deposition during the current Holocene highstand (A) and the Last Glacial Maximum (B). C. The occurrence of an elongated area of non-deposition adjacent to contourite deposits on the Malta Plateau indicates the path of bottom currents flowing at around 100 m w.d.

descending shelf-edge trajectory of the clinothems bracketed between ES1 and ES8 unconformities; ii) no evidence of relevant tectonic activity after the MPT (Fig. 12). ES1-ES8 unconformities therefore represent the sequence boundaries formed until the end of each eustatic fall (Fig. 6B). Independently constrained calibration of the youngest (ES1) and oldest (ES8) unconformities, dated at 30 kyr BP (Kuhlmann et al., 2015) and ca. 800 ka (Di Stefano et al., 1993), respectively, support this interpretation (Fig. 6B). Clinothems above the sequence boundaries show onlap terminations on the slope and have erosional topsets (highlighted by topset terminations; Fig. 6A), and correlative MTDs in the basin and on the slope, here named clinothem-related MTDs (Fig. 14B). The erosional nature of their topsets can be explained by a fluvial system docked at the shelf edge, as documented in tank experiments (Martin et al., 2009). The depths of the rollover points of each sequence boundary indicate a quasi-steady subsidence rate of 0.1 mm/yr (Fig. 6B) and suggest, like in the western Adriatic Sea (Maselli et al., 2010), the formation of these erosional surfaces by subaerial exposure as reported in Kuhlmann et al. (2015) in the adjacent study area. However, the presence of ES1 rollover point at 200 m w. d. on the Malta Plateau (Figs. 6A, 8) and 75 m below the position of sea level during the last eustatic lowstand, would imply a subsidence rate of 2.5 mm/yr solely in the last 30 kyr. Instead, we suggest that ES1 can be the result of subaerial erosion during the last lowstand on the inner and mid shelf and of subaqueous erosion on the outer shelf, presumably by waves and bottom currents (Fig. 14B). The subaqueous erosion on the outer shelf may have further contributed to the emplacement of MTDs in the basin (Fig. 14B). The clinothems prograded at the shelf edge until further sea-level rise brought about the flooding of the continental shelf. During flooding phases and highstands, the shoreline shifted landward accompanied by: i) the formation of a condensed succession in the basin detected as single and laterally continuous reflections observed in MCS profiles (Fig. 14A). These reflections can be interpreted as hemipelagites and shelf-derived sediments as reported elsewhere in similar contexts (e.g. Paumard et al., 2020); ii) the deposition of sediment drifts on the outer shelf (Fig. 14A and C). We indeed found evidence of contourite deposits as shallow as 100 m w.d. on the Malta Plateau (inset of Fig. 8), similar to those suggested close to Malta by Micallef et al. (2013) (Fig. 1). We thus infer the presence of bottom currents constrained in their paths by the structural highs of the Malta Plateau during highstands suggesting an along-contour sediment redistribution, under the influence of the MAW from north to south along the shelf edge (Fig. 14C). Overall, this evidence suggest that sea level was the main driver in determining the position of the depocenters with a systematic shift of the depocenters towards the shelf edge during glacial periods. Therefore, sea-level variations concur in promoting margin destabilization under high-amplitude glacio-eustatic fluctuations (Fig. 12). This implies orbitally-controlled climatic cycles as the key predisposing factor of margin instability after the MPT, with clinothem-MTDs paced roughly at 100 kyr cycles (Table 4).

## 6. Conclusions

The Pliocene–Quaternary stratigraphic succession of the Gela Basin results from the stacking of three main types of sedimentary bodies: clinothems, contourite deposits and mass-transport deposits (MTDs). Altogether, the stratal stacking pattern records variations in tectonic activity, climate (affecting sediment flux from the continent and eustasy), and changes in the oceanographic regime at Milankovitch and sub-Milankovitch time scales.

Tectonic-related MTDs are the least recurrent gravity-flow deposits in the Gela Basin but the largest in volumes until the Lower Pleistocene in the north of the basin. The outbuilding of the margin changed drastically along the Middle Pleistocene Transition (MPT, 0.8 Ma) from a shelf-edge progradational phase with an accumulation of 700 m in ca. 4.5 Myr, to a progradational-aggradational phase with a comparable volume of sediment accumulated in a much shorter time span. This high

sediment accumulation rate promoted the emplacement of MTDs favoured by significantly increased slope gradients of the foresets of prograding clinofolds. Therefore, shelf-edge clinothems and their associated MTDs were paced at Milankovitch cyclicity and resulted in the systematic shift of the shoreline to the shelf edge during glacial periods, revealing sea-level change as the main driver in determining the position of the depocenters along the shelf-edge and indirectly favoring margin destabilization after the MPT.

Following the MPT, contourite deposits, confined to the lower slope since the Upper Pliocene, progressively migrated upslope, under the action of enhanced bottom currents with a flow pattern likely similar to that of the modern LIW. Contourite drifts formed on the up and down-current side of a shelf-edge headland inherited from the Pre-Pliocene morphology of the margin, which probably accelerated bottom currents locally. Markedly different sediment accumulation rates north and south along the margin during interglacial periods (e.g. MIS 5) further suggest a re-organization in the sediment dispersal along the shelf, with sediment by-pass around the shelf-edge headland. In this context, MTDs generated from failed, contourite deposits are systematically found above erosional surfaces, which probably acted as glide planes.

Overall, these findings suggest that:

1. The contourite- and clinothem-related MTDs are smaller in size compared to the tectonic-related MTDs but more recurrent and reflect sea-level fluctuations, changes in sediment supply and dispersal by bottom currents.
2. Contourite deposits emplaced over erosional unconformities are prone to failure thereby acting as a major control on the architecture of the margin.
3. The physical scale of the lithosomes recorded in the stratigraphic succession has no implications on the time elapsed during their deposition, as already observed in other margins.

## CRedit authorship contribution statement

**Tugdual Gauchery:** Investigation, Visualization, Software, Writing - original draft. **Marzia Rovere:** Conceptualization, Methodology, Writing - original draft, Writing - review & editing, Supervision. **Claudio Pellegrini:** Conceptualization, Methodology, Writing - original draft, Writing - review & editing. **Antonio Cattaneo:** Methodology, Supervision. **Elisabetta Campiani:** Data curation, Software. **Fabio Trincardi:** Writing - review & editing.

## Declaration of competing interest

The authors declare that they have no known competing financial interests or personal relationships that could have appeared to influence the work reported in this paper.

## Acknowledgments

The authors wish to thank Eni S.p.A., in particular Luca Aleotti and Alessandro Fattorini for granting the access to the virtual data room at their premises in San Donato Milanese (Italy) and Claudio Cattaneo for his kind technical assistance. Alessandra Asioli helped to interpret the biozones of the boreholes. Francesca Zolezzi helped a lot in putting together and analysing the seismic data during T.G.'s several stays at Rina Consulting S.p.A. The comments and suggestions by Victorien Paumard, Andrew S. Madof and Tiago M. Alves greatly improved the paper. The PhD of Tugdual Gauchery is funded by the European Union's Horizon 2020 research and innovation programme under the Marie-Sklodowska-Curie grant via project ITN SLATE (grant agreement No 721403). This work is dedicated to the memory of our beloved colleague Elisabetta Campiani.

## References

- Alves, T.M., 2010. A 3-D morphometric analysis of erosional features in a contourite drift from offshore SE Brazil. *Geophys. J. Int.* 183 (3), 1151–1164. <https://doi.org/10.1111/j.1365-246X.2010.04827.x>.
- Alves, T.M., Gamboa, D., 2019. Mass-transport deposits as markers of local tectonism in extensional basins. In: Ogata, K., Festa, A., Pini, G.A. (Eds.), *Submarine Landslides Subaqueous Mass Transport Deposits from Outcrops to Seismic Profiles*. Geoph. Monog. Series 246. AGU, pp. 71–90. <https://doi.org/10.1002/978111990513.ch5>.
- Amelio, M., Martorelli, E., 2008. Seismo-stratigraphic characters of paleocontourites along the calabro-tyrrhenian margin (southern Tyrrhenian Sea). *Mar. Geol.* 252, 141–149. <https://doi.org/10.1016/j.margeo.2008.03.011>.
- Anell, I., Midtkandal, I., 2017. The quantifiable clinothem – types, shapes and geometric relationships in the Plio-Pleistocene Giant Foresets Formation, Taranaki Basin, New Zealand. *Basin Res.* 29 (S1), 277–297. <https://doi.org/10.1111/bre.12149>.
- Argnani, A., 1987. The Gela nappe: evidence of accretionary melange in the maghrebian foredeep of sicily. *Memorie Società Geologica Italiana* 38, 419–428.
- Argnani, A., Torelli, L., 2001. The Pelagian Shelf and its graben system (Italy/Tunisia). *Memoir. Mus. Natl. Hist.* 186, 529–544.
- Astraldi, M., Gasparini, G.P., Gervasio, L., Salusti, E., 2001. Dense water dynamics along the Strait of sicily (Mediterranean Sea). *J. Phys. Oceanogr.* 31, 3457–3475. [https://doi.org/10.1175/1520-0485\(2001\)031<3457:DWDATS>2.0.CO;2](https://doi.org/10.1175/1520-0485(2001)031<3457:DWDATS>2.0.CO;2).
- Béranger, K., Mortier, L., Gasparini, G.P., Zarudkio, E.F.K., Astraldi, M., Crépon, M., 2004. The dynamics of the Sicily Strait: a comprehensive study from observations and models. *Deep-Sea Res. Pt. II* 51 (4–5), 411–440. <https://doi.org/10.1016/j.dsr2.2003.08.004>.
- Bishop, W.F., Debono, G., 1996. The hydrocarbon geology of southern offshore Malta and surrounding regions. *J. Petrol. Geol.* 19, 129–160. <https://doi.org/10.1111/j.1747-5457.1996.tb00422.x>.
- Brackenridge, R., Stow, D.A.V., Hernández-Molina, F.J., 2011. Contourites within a deep-water sequence stratigraphic framework. *Geo Mar. Lett.* 31, 343–360. <https://doi.org/10.1007/s00367-011-0256-9>.
- Butler, R.W.H., Grasso, M., La Manna, F., 1992. Origin and deformation of the neogene-maghrebian foredeep at the Gela nappe, SE sicily. *J. Geol. Soc.* 149 (4), 547–556. <https://doi.org/10.1144/gsjgs.149.4.0547>.
- Colantoni, P., Del Monte, M., Gallignani, P., Zarudkio, E.F.K., 1975. Il Banco Graham: un vulcano recente del Canale di Sicilia. *Giorn. Geol.* 40, 141–162.
- Di Stefano, E., Infuso, S., Scarantino, S., 1993. Plio-Pleistocene sequence stratigraphy of south western offshore Sicily from well logs and seismic sections in a high resolution calcareous plankton biostratigraphic framework. In: Max, M.D., Colantoni, P. (Eds.), *Geological Development of the Sicilian-Tunisian Platform*. Reports in Marine Science, vol. 58. UNESCO, pp. 37–42.
- EMODnet Bathymetry Consortium, 2016. EMODnet Digital Bathymetry (DTM). The European Marine Observation and Data Network. <https://doi.org/10.12770/c7b53704-999d-4721-b1a3-04ec60c87238>.
- Ercilla, G., Farran, M., Alonso, B., Diaz, J.I., 1994. Pleistocene progradational growth pattern of the northern Catalonia continental shelf (northwestern Mediterranean). *Geo Mar. Lett.* 14, 264–271. <https://doi.org/10.1007/BF01274062>.
- Falcini, F., Martorelli, E., Chiochi, F.L., Salusti, E., 2016. A general theory for the effect of local topographic unevenness on contourite deposition around marine capes: an inverse problem applied to the Italian continental margin (Cape Suvero). *Mar. Geol.* 378, 74–80. <https://doi.org/10.1016/j.margeo.2016.01.004>.
- Fatoke, O.A., Bhattacharya, J.P., 2010. Controls on depositional systems and sequence stratigraphy of the Pliocene-Pleistocene strata of eastern Niger delta, Nigeria. AAPG (Am. Assoc. Pet. Geol.) Convention, Denver, Colorado. June 7-10, 2009. [http://www.searchanddiscovery.com/documents/2010/10220fatoke/ndx\\_fatoke.pdf](http://www.searchanddiscovery.com/documents/2010/10220fatoke/ndx_fatoke.pdf).
- Faugères, J.C., Stow, D.A.V., Imbert, P., Viana, A., 1999. Seismic features diagnostic of contourite drifts. *Mar. Geol.* 162, 1–38. [https://doi.org/10.1016/S0025-3227\(99\)00068-7](https://doi.org/10.1016/S0025-3227(99)00068-7).
- Finetti, I., 1984. Geophysical study of the sicily channel rift zone. *Boll. Geofis. Teor. Appl.* 26, 3–28.
- García-Castellanos, D., Estrada, F., Jiménez-Munt, I., Gorini, C., Fernández, M., Vergés, J., De Vicente, R., 2009. Catastrophic flood of the Mediterranean after the Messinian salinity crisis. *Nature* 462, 778–781. <https://doi.org/10.1038/nature08555>.
- Gardiner, W., Grasso, M., Sedgely, D., 1993. Plio-Pleistocene stratigraphy and recent movements of the Malta platform. In: Max, M.D., Colantoni, P. (Eds.), *Geological Development of the Sicilian-Tunisian Platform*. Reports in Marine Science, vol. 58. UNESCO, pp. 111–116.
- Gardiner, W., Grasso, M., Sedgely, D., 1995. Plio-pleistocene fault movement as evidence for mega-block kinematics within the Hyblean—Malta Plateau, Central Mediterranean. *J. Geodyn.* 19, 35–51. [https://doi.org/10.1016/0264-3707\(94\)00006-9](https://doi.org/10.1016/0264-3707(94)00006-9).
- Ghielmi, M., Amore, M.R., Bolla, E.M., Carubelli, P., Knezaurek, G., Serrano, C., 2012. The Pliocene to pleistocene succession of the hyblean foredeep (sicily, Italy). October 23-26, 2011 AAPG (Am. Assoc. Pet. Geol.) Internat. Conf. Exhib. Milan, Italy. [http://www.searchanddiscovery.com/documents/2012/30220ghielmi/ndx\\_ghielmi.pdf](http://www.searchanddiscovery.com/documents/2012/30220ghielmi/ndx_ghielmi.pdf).
- Ghisetti, F.C., Gorman, A.R., Grasso, M., Vezzani, L., 2009. Imprint of foreland structure on the deformation of a thrust sheet: the Plio-Pleistocene Gela nappe (southern Sicily, Italy). *Tectonics* 28, 1–16. <https://doi.org/10.1029/2008TC002385>.
- Gibbard, P.L., Head, M.J., Walker, M.J.C., 2010. The subcommission on quaternary stratigraphy, formal ratification of the quaternary system/period and the pleistocene series/epoch with a base at 2.58 Ma. *J. Quat. Sci.* 25 (2), 96–102. <https://doi.org/10.1002/jqs.1338>.
- Gong, C., Steel, R.J., Wang, Y., Lin, C., Olariu, C., 2016. Shelf-margin architecture variability and its role in sediment-budget partitioning into deep-water areas. *Earth Sci. Rev.* 154, 72–101. <https://doi.org/10.1016/j.earscirev.2015.12.003>.
- Gong, C., Blum, M.D., Wang, Y., Lin, C., Xu, Q., 2018. Can climatic signals be discerned in a deep-water sink?: an answer from the Pearl River source-to-sink sediment-routing system. *Geol. Soc. Am. Bull.* 130, 661–677. <https://doi.org/10.1130/B31578.1>.
- Haile, N.S., 1987. Time and age in geology the use of Upper/Lower, late/early in stratigraphic nomenclature. *Mar. Petrol. Geol.* 4, 255–257. [https://doi.org/10.1016/0264-8172\(87\)90048-1](https://doi.org/10.1016/0264-8172(87)90048-1).
- Holland-Hansen, W., Martinsen, O.J., 1996. Shoreline trajectories and sequences: description of variable depositional-dip scenarios. *J. Sediment. Res.* 66, 670–688. <https://doi.org/10.1306/d42683dd-2b26-11d7-8648000102c1865d>.
- Henriquet, M., Dominguez, S., Barreca, G., Malavielle, J., Monaco, C., 2020. Structural and tectono-stratigraphic review of the Sicilian orogen and new insights from analogue modeling. *Earth Sci. Rev.* 208, 103257. <https://doi.org/10.1016/j.earscirev.2020.103257>.
- Hunt, D., Tucker, M.E., 1992. Stranded parasequences and the forced regressive wedge systems tract: deposition during base-level fall. *Sediment. Geol.* 81, 1–9. [https://doi.org/10.1016/0037-0738\(92\)90052-S](https://doi.org/10.1016/0037-0738(92)90052-S).
- Johannessen, E.P., Steel, R.J., 2005. Shelf-margin clinoforms and prediction of deepwater sands. *Basin Res.* 17, 521–550. <https://doi.org/10.1111/j.1365-2117.2005.00278.x>.
- Kuhlmann, J., Asioli, A., Trincardi, F., Klügel, A., Huhn, K., 2015. Sedimentary response to Milankovitch-type climatic oscillations and formation of sediment undulations: evidence from a shallow-shelf setting at Gela Basin on the Sicilian continental margin. *Quat. Sci. Rev.* 108, 76–94. <https://doi.org/10.1016/j.quascirev.2014.10.030>.
- Kuhlmann, J., Asioli, A., Trincardi, F., Klügel, A., Huhn, K., 2017. Landslide frequency and failure mechanisms at NE Gela Basin (Strait of sicily). *J. Geophys. Res.-Sol. Ea.* 122, 2223–2243. <https://doi.org/10.1002/2017JF004251>.
- Laberg, J.S., Camerlenghi, A., 2008. The significance of contourites for submarine slope stability. In: Rebesco, M., Camerlenghi, A. (Eds.), *Contourites*. Developments in Sedimentology 60. Elsevier Science, pp. 537–556. [https://doi.org/10.1016/S0070-4571\(08\)10025-5](https://doi.org/10.1016/S0070-4571(08)10025-5).
- Lermusiaux, P.F.J., Robinson, A.R., 2001. Features of dominant mesoscale variability, circulation patterns and dynamics in the Strait of Sicily. *Deep-Sea Res. Pt. I* 48 (9), 1953–1997. [https://doi.org/10.1016/S0967-0637\(00\)00114-X](https://doi.org/10.1016/S0967-0637(00)00114-X).
- Lirer, F., Foresi, L.M., Iaccarino, S.M., Salvatore, G., Turco, E., Cosentino, C., Sierro, F.J., Caruso, A., 2019. Mediterranean Neogene planktonic foraminifer biozonation and Biochronology. *Earth Sci. Rev.* 196, 102869. <https://doi.org/10.1016/j.earscirev.2019.05.013>.
- Llave, E., Matias, H., Hernández-Molina, F.J., Ercilla, G., Stow, D.A.V., Medialdea, T., 2011. Pliocene-Quaternary contourites along the northern Gulf of Cadiz margin: sedimentary stacking pattern and regional distribution. *Geo Mar. Lett.* 31, 377–390. <https://doi.org/10.1007/s00367-011-0241-3>.
- Madof, A.S., Christie-Blick, N., Anders, M.H., Febo, L.A., 2017. Unreciprocated sedimentation along a mud-dominated continental margin, Gulf of Mexico, USA: implications for sequence stratigraphy in muddy settings devoid of depositional sequences. *Mar. Petrol. Geol.* 80, 492–516. <https://doi.org/10.1016/j.marpetgeo.2016.12.022>.
- Madof, A.S., Harris, A.D., Baumgardner, S.E., Sadler, P.M., Laugier, F.J., Christie-Blick, N., 2019. Stratigraphic aliasing and the transient nature of deep-water depositional sequences: revisiting the Mississippi Fan. *Geology* 47 (6), 545–549. <https://doi.org/10.1130/G46159.1>.
- Marani, M., Argnani, A., Roveri, M., Trincardi, F., 1993. Sediment drifts and erosional surfaces in the central Mediterranean: seismic evidence of bottom-current activity. *Sediment. Geol.* 82, 207–220. [https://doi.org/10.1016/0037-0738\(93\)90122-L](https://doi.org/10.1016/0037-0738(93)90122-L).
- Martin, J., Paola, C., Abreu, V., Neal, J., Sheets, B., 2009. Sequence stratigraphy of experimental strata under known conditions of differential subsidence and variable base level. AAPG (Am. Assoc. Pet. Geol.) Bull. 93 (4), 503–533. <https://doi.org/10.1306/12110808057>.
- Martinelli, M., Bistacchi, A., Balsamo, F., Meda, M., 2019. Late Oligocene to Pliocene extension in the Maltese islands and implications for geodynamics of the Pantelleria rift and pelagian platform. *Tectonics* 38, 3394–3415. <https://doi.org/10.1029/2019TC005627>.
- Martorelli, E., Petroni, G., Chiochi, F.L., 2011. Contourites offshore Pantelleria Island (sicily channel, Mediterranean Sea): depositional, erosional and biogenic elements. *Geo Mar. Lett.* 31, 481–493. <https://doi.org/10.1007/s00367-011-0244-0>.
- Martorelli, E., Bosman, A., Casalbone, D., Falcini, F., 2016. Interaction of down-slope and along-slope processes off Capo Vaticano (southern Tyrrhenian Sea, Italy), with particular reference to contourite-related landslides. *Mar. Geol.* 378, 43–55. <https://doi.org/10.1016/j.margeo.2016.01.005>.
- Maselli, V., Trincardi, F., Cattaneo, A., Ridente, D., Asioli, A., 2010. Subsidence pattern in the central Adriatic and its influence on sediment architecture during the last 400 kyr. *J. Geophys. Res.-Sol. Ea.* 115, B12106. <https://doi.org/10.1029/2010JB007687>.
- McCave, I.N., Hall, I.R., 2006. Size sorting in marine muds: processes, pitfalls, and prospects for paleoflow-speed proxies. *G-cubed* 7, Q10N05. <https://doi.org/10.1029/2006GC001284>.
- Miall, A.D., 2016. The evaluation of unconformities. *Earth Sci. Rev.* 163, 22–71. <https://doi.org/10.1016/j.earscirev.2016.09.011>.
- Micallef, A., Fogliani, F., Le Bas, T., Angeletti, L., Maselli, V., Pasuto, A., Taviani, M., 2013. The submerged paleolandscape of the Maltese Islands: morphology, evolution and relation to Quaternary environmental change. *Mar. Geol.* 335, 129–147. <https://doi.org/10.1016/J.MARGE0.2012.10.017>.

- Minisini, D., Trincardi, F., 2009. Frequent failure of the continental slope: the Gela Basin (sicily channel). *J. Geophys. Res.-Earth* 114, 1–17. <https://doi.org/10.1029/2008JF001037>.
- Minisini, D., Trincardi, F., Asioli, A., Canu, M., Fogliani, F., 2007. Morphologic variability of exposed mass-transport deposits on the eastern slope of Gela Basin (Sicily channel). *Basin Res.* 19, 217–240. <https://doi.org/10.1111/j.1365-2117.2007.00324.x>.
- Miramontes, E., Cattaneo, A., Jouet, G., Théreau, E., Thomas, Y., Rovere, M., Cauquil, E., Trincardi, F., 2016. The pianosa contourite depositional system (northern Tyrrhenian Sea): drift morphology and plio-quaternary stratigraphic evolution. *Mar. Geol.* 378, 20–42. <https://doi.org/10.1016/j.margeo.2015.11.004>.
- Miramontes, E., Garziglia, S., Sultan, N., Jouet, G., Cattaneo, A., 2018. Morphological control of slope instability in contourites: a geotechnical approach. *Landslides* 15, 1085–1095. <https://doi.org/10.1007/s10346-018-0956-6>.
- Mitchum Jr., R.M., Vail, P.R., Sangree, J.B., 1977. Seismic stratigraphy and global changes of sea level, Part 6: stratigraphic interpretation of seismic reflection patterns in depositional sequences, section 2: application of seismic reflection configuration to stratigraphic interpretation. AAPG (Am. Assoc. Pet. Geol.) Memoir 26, 117–133. <https://doi.org/10.1306/M26490C8>.
- Mulder, T., Faugères, J.-T., Gonthier, E., 2008. Mixed turbidite-contourite systems. In: Rebecco, M., Camerlenghi, A. (Eds.), *Contourites. Developments in Sedimentology* 60. Elsevier, pp. 435–456. [https://doi.org/10.1016/S0070-4571\(08\)10021-8](https://doi.org/10.1016/S0070-4571(08)10021-8).
- Patrino, S., Helland-Hansen, W., 2018. Clinoform systems: review and dynamic classification scheme for shorelines, subaqueous deltas, shelf-edges and continental margins. *Earth Sci. Rev.* 185, 202–233. <https://doi.org/10.1016/j.earscirev.2018.05.016>.
- Paumard, V., Bourget, J., Payenberg, T., George, A.D., Ainsworth, R.B., Lang, S., 2019. From quantitative 3D seismic stratigraphy to sequence stratigraphy: insights into the vertical and lateral variability of shelf-margin depositional systems at different stratigraphic orders. *Mar. Petrol. Geol.* 110, 797–831. <https://doi.org/10.1016/j.marpetgeo.2019.07.007>.
- Paumard, V., Bourget, J., Payenberg, T., George, A.D., Ainsworth, R.B., Lang, S., Posamentier, H.W., 2020. Controls on deep-water sand delivery beyond the shelf edge: accommodation, sediment supply, and deltaic process regime. *J. Sediment. Res.* 90 (1), 104–130. <https://doi.org/10.2110/jsr.2020.2>.
- Pearson, P.N., Wade, B.S., Backman, J., Raffi, I., Monechi, S., 2017. Sub-series and sub-epochs are informal units and should continue to be omitted from the International Chronostratigraphic Chart. *Episodes* 40 (1), 5–7. <https://doi.org/10.18814/epiugs/2017/v40i1/017002>.
- Pellegrini, C., Maselli, V., Trincardi, F., 2016. Pliocene–Quaternary contourite depositional system along the south-western Adriatic margin: changes in sedimentary stacking pattern and associated bottom currents. *Geo Mar. Lett.* 36, 67–79. <https://doi.org/10.1007/s00367-015-0424-4>.
- Pellegrini, C., Maselli, V., Gamberi, F., Asioli, A., Bohacs, K.M., Drexler, T.M., Trincardi, F., 2017a. How to make a 350-m-thick lowstand systems tract in 17,000 years: the Late Pleistocene Po River (Italy) lowstand wedge. *Geology* 45 (4), 327–330. <https://doi.org/10.1130/G38848.1>.
- Pellegrini, C., Bohacs, K.M., Drexler, T.M., Gamberi, F., Rovere, M., Trincardi, F., 2017b. Identifying the sequence boundary in over- and under-supplied contexts: the case of the late Pleistocene adriatic continental margin. In: Hart, B., Rosen, N.C., West, D., D'Agostino, A., Messina, C., Hoffman, M., Wild, R. (Eds.), *Sequence Stratigraphy: the Future Defined. Proceedings of the 36<sup>th</sup> Annual Perkins-Rosen Research Conference*, pp. 160–182. <https://doi.org/10.5724/gcs.17.160>. Houston, Texas.
- Pellegrini, C., Patrino, S., Helland-Hansen, W., Steel, R.J., Trincardi, F., 2020. Clinoforms and clinothems: fundamental elements of basin infill. *Basin Res.* 32, 187–205. <https://doi.org/10.1111/bre.12446>.
- Pena, L.D., Goldstein, S.L., 2014. Thermohaline circulation crisis and impacts during the mid-Pleistocene transition. *Science* 345, 318–322. <https://doi.org/10.1126/science.1249770>.
- Pirmez, C., Pratson, L.F., Steckler, M.S., 1998. Clinoform development by advection-diffusion of suspended sediment: modeling and comparison to natural systems. *J. Geophys. Res.-Sol. Ea.* 103, 24141–24157. <https://doi.org/10.1029/98jb01516>.
- Posamentier, H.W., Allen, G.P., James, D.P., Tesson, M., 1992. Forced regressions in a sequence stratigraphic framework: concepts, examples, and exploration significance (1). AAPG (Am. Assoc. Pet. Geol.) Bull. 76, 1687–1709. <https://doi.org/10.1306/BDF8AA6-1718-11D7-8645000102C1865D>.
- Reeder, M.S., Rothwell, G., Stow, D.A.V., 2002. The Sicilian gateway: anatomy of the deep-water connection between East and West Mediterranean basins. *Geol. Soc. Mem.* 22, 171–189. <https://doi.org/10.1114/GSL.MEM.2002.022.01.13>.
- Rich, J.L., 1951. Three critical environments of deposition, and criteria for recognition of rocks deposited in each of them. *GSA Bull.* 62, 1–20. [https://doi.org/10.1130/0016-7606\(1951\)62\[1:TCEODA\]2.0.CO](https://doi.org/10.1130/0016-7606(1951)62[1:TCEODA]2.0.CO) accessed day=2.
- Roque, C., Duarte, H., Terrinha, P., Valadares, V., Noiva, J., Cachão, M., Ferreira, J., Legoinha, P., Zitellini, N., 2012. Pliocene and Quaternary depositional model of the Algarve margin contourite drifts (Gulf of Cadiz, SW Iberia): seismic architecture, tectonic control and paleoceanographic insights. *Mar. Geol.* 303–306, 42–62. <https://doi.org/10.1016/j.margeo.2011.11.001>.
- Rovere, M., Pellegrini, C., Chiggiato, J., Campiani, E., Trincardi, F., 2019. Impact of dense bottom water on a continental shelf: an example from the SW Adriatic margin. *Mar. Geol.* 408, 123–143. <https://doi.org/10.1016/j.margeo.2018.12.002>.
- Smith, D.G., Bailey, R.J., Burgess, P.M., Fraser, A.J., 2015. Strata and time: probing the gaps in our understanding. *Geol. Soc. Spec. Publ.* 404 (1), 1–10. <https://doi.org/10.1144/SP404.16>.
- Somoza, L., Hernández-Molina, F.J., De Andres, J.R., Rey, J., 1997. Continental shelf architecture and sea-level cycles: late Quaternary high-resolution stratigraphy of the Gulf of Cádiz, Spain. *Geo Mar. Lett.* 17, 133–139. <https://doi.org/10.1007/s003670050018>.
- Spratt, R.M., Lisiecki, L.E., 2006. A late Pleistocene sea level stack. *Clim. Past* 12, 1079–1092. <https://doi.org/10.5194/cp-12-1079-2006>.
- Steckler, M.S., Mountain, G.S., Miller, K.G., Christie-Blick, N., 1998. Reconstruction of Tertiary progradation and clinoform development on the New Jersey passive margin by 2-D backstripping. *Mar. Geol.* 154, 399–420. [https://doi.org/10.1016/S0025-3227\(98\)00126-1](https://doi.org/10.1016/S0025-3227(98)00126-1).
- Steel, R., Olsen, T., 2002. Clinoforms, clinoform trajectories and deepwater sands. In: Armentrout, J.M., Rosen, N.C. (Eds.), *Sequence Stratigraphic Models for Exploration and Production: Evolving Methodology, Emerging Models, and Application Histories. Proceedings of 22<sup>nd</sup> Annual Gulf Coast Section SEPM Foundation Bob F. Perkins Research Conference*, pp. 367–380. <https://doi.org/10.5724/gcs.02.22.0367>. Houston, Texas.
- Stoker, M.S., Hafidason, H., 2005. Contourites and their relevance for mass wasting along the Mid-Norwegian Margin. *Mar. Petrol. Geol.* 22, 85–96. <https://doi.org/10.1016/j.marpetgeo.2004.10.012>.
- Stow, D.A.V., Faugères, J.-C., 2008. Contourite facies and the facies model. In: Rebecco, M., Camerlenghi, A. (Eds.), *Contourites. Developments in Sedimentology* 60. Elsevier Science, pp. 223–256. [https://doi.org/10.1016/S0070-4571\(08\)10013-9](https://doi.org/10.1016/S0070-4571(08)10013-9).
- Stow, D.A.V., Hernández-Molina, F.J., Llave, E., Sayago-Gil, M., Díaz-del Río, V., Branson, A., 2009. Bedform-velocity matrix: the estimation of bottom current velocity from bedform observations. *Geology* 37, 327–330. <https://doi.org/10.1130/G25259A.1>.
- Thiéblemont, A., Hernández-Molina, F.J., Miramontes, E., Raison, F., Penven, P., 2019. Contourite depositional systems along the Mozambique channel: the interplay between bottom currents and sedimentary processes. *Deep-Sea Res. Pt. I* 147, 79–99. <https://doi.org/10.1016/j.dsr.2019.03.012>.
- Thöle, H., Kuhlmann, G., Lutz, R., Gaedicke, C., 2016. Late Cenozoic submarine slope failures in the southern North Sea - evolution and controlling factors. *Mar. Petrol. Geol.* 75, 272–290. <https://doi.org/10.1016/j.marpetgeo.2016.04.028>.
- Toucanne, S., Jouet, G., Ducassou, E., Bassetti, M.A., Dennielou, B., Angue Minto'o, C.M., Lahmi, M., Touyet, N., Charlier, K., Lericola, G., Mulder, T., 2012. A 130,000-year record of levantine intermediate water flow variability in the Corsica Trough, western Mediterranean Sea. *Quat. Sci. Rev.* 33, 55–73. <https://doi.org/10.1016/j.quascirev.2011.11.020>.
- Trincardi, F., Argani, A., 1990. Gela submarine slide: a major basin-wide event in the Plio-quaternary foredeep of Sicily. *Geo Mar. Lett.* 10, 13–21. <https://doi.org/10.1007/BF02431017>.
- Tziperman, E., Gildor, H., 2003. On the mid-Pleistocene transition to 100-kyr glacial cycles and the asymmetry between glaciation and deglaciation times. *Paleoceanography* 18 (1), 1001. <https://doi.org/10.1029/2001PA000627>.
- Urlaub, M., Talling, P.J., Masson, D.G., 2013. Timing and frequency of large submarine landslides: implications for understanding triggers and future geohazard. *Quat. Sci. Rev.* 72, 63–82. <https://doi.org/10.1016/j.quascirev.2013.04.020>.
- Van Rooij, D., Iglesias, J., Hernández-Molina, F.J., Ercilla, G., Gomez-Ballesteros, M., Casas, D., Llave, E., De Hauwere, A., Garcia-Gil, S., Acosta, J., Henriot, J.P., 2010. The le danois contourite depositional system: interactions between the mediterranean Outflow water and the upper cantabrian slope (north iberian margin). *Mar. Geol.* 274, 1–20. <https://doi.org/10.1016/j.margeo.2010.03.001>.
- Vandorpe, T.P., Van Rooij, D., Stow, D.A.V., Henriot, J.-P., 2011. Pliocene to Recent shallow-water contourite deposits on the shelf and shelf edge off south-western Mallorca, Spain. *Geo Mar. Lett.* 31, 391–403. <https://doi.org/10.1007/s00367-011-0248-9>.
- Verdicchio, G., Trincardi, F., 2008a. Mediterranean shelf-edge muddy contourites: examples from the Gela and south adriatic basins. *Geo Mar. Lett.* 28, 137–151. <https://doi.org/10.1007/s00367-007-0096-9>.
- Verdicchio, G., Trincardi, F., 2008b. Shallow-water contourites. In: Rebecco, M., Camerlenghi, A. (Eds.), *Contourites. Developments in Sedimentology* 60. Elsevier Science, pp. 409–433. [https://doi.org/10.1016/S0070-4571\(08\)10020-6](https://doi.org/10.1016/S0070-4571(08)10020-6).